MNRAS **000**, 1–18 (2017) Preprint 29 January 2022 Compiled using MNRAS LATEX style file v3.0

On the nature of the luminous Lyα emitter CR7 and its UV components: physical conditions and *JWST* predictions⋆

David Sobral[1,2]†, Jorryt Matthee[2], Gabriel Brammer[3], Andrea Ferrara[4,5], Lara Alegre[6] Huub Röttgering[2], Daniel Schaerer[7,8], Bahram Mobasher[9], Behnam Darvish[10]
[1] *Department of Physics, Lancaster University, Lancaster, LA1 4YB, UK*
[2] *Leiden Observatory, Leiden University, P.O. Box 9513, NL-2300 RA Leiden, The Netherlands*
[3] *Space Telescope Science Institute, 3700 San Martin Dr, Baltimore MD 21211, USA*
[4] *Scuola Normale Superiore, Piazza dei Cavalieri 7, I-56126 Pisa, Italy*
[5] *Kavli IPMU, The University of Tokyo, 5-1-5 Kashiwanoha, Kashiwa 277-8583, Japan*
[6] *Institute for Astronomy, University of Edinburgh, Royal Observatory, Blackford Hill, Edinburgh EH9 3HJ, UK*
[7] *Observatoire de Genève, UniversitŐ de GenŔve, 51 Ch. des Maillettes, 1290 Versoix, Switzerland*
[8] *CNRS, IRAP, 14 Avenue E. Belin, 31400 Toulouse, France*
[9] *Department of Physics and Astronomy, University of California, 900 University Ave., Riverside, CA 92521, USA*
[10] *Cahill Center for Astrophysics, California Institute of Technology, 1216 East California Boulevard, Pasadena, CA 91125, USA*

arXiv:1710.08422v1 [astro-ph.GA] 23 Oct 2017

29 January 2022

ABSTRACT

We present new *HST*/WFC3 grism observations and re-analyse VLT data to unveil the continuum, variability and rest-frame UV lines of the three UV components of the most luminous Lyα emitter at $z = 6.6$, COSMOS Redshift 7 (CR7; Sobral et al. 2015). Our re-reduced, flux calibrated X-SHOOTER spectra of CR7 reveal a tentative detection of HeII with $F_{HeII} = (1.8\pm0.7)\times10^{-17}$ erg s^{-1} cm^{-2} and we identify the signal ($\sim 2.6\,\sigma$) as coming only from observations obtained along the major axis of Lyα emission. There is a change of +0.2-0.5 mag in UltraVISTA J band data for CR7 from DR2 to DR3, which virtually eliminates the strong J-band excess previously interpreted as being caused by HeII. Our WFC3 grism spectra provide a significant detection of the UV continuum of CR7's clump A, yielding an excellent fit to a power law with $\beta = -2.4\pm0.4$ and $M_{UV} = -21.7\pm0.3$, consistent with no variability. *HST* grism data fail to detect any rest-frame UV line in clump A above $3\,\sigma$, yielding $F_{HeII} < 0.5\times10^{-17}$ erg s^{-1} cm^{-2} (EW$_0$ < 10 Å) at a 95% confidence level. Clump C is tentatively identified as a potential variable and high ionisation source with $F_{HeII} = (1.0 \pm 0.4) \times 10^{-17}$ erg s^{-1} cm^{-2}. We perform CLOUDY modelling to constrain the metallicity and the ionising nature of CR7, and also make emission-line predictions for *JWST*/NIRSpec. CR7 seems to be actively forming stars without any clear AGN activity in clumps A and B, consistent with a metallicity of $\sim 0.05 - 0.2\,Z_\odot$ and with component A experiencing the most massive starburst. Component C may host a high ionisation source/AGN. Our results highlight the need for spatially resolved information to study the complex formation and assembly of early galaxies within the epoch of re-ionisation.

Key words: Galaxies: high-redshift; evolution; ISM; cosmology: observations; reionization.

1 INTRODUCTION

Thanks to significant progress in identifying large samples of distant galaxies, detailed studies of the properties of the earliest stellar populations and black holes are now possible. Studies based on the UV slopes (β) of high redshift galaxies indicate that they are consistent with little dust (e.g. Dunlop et al. 2012; Bouwens et al. 2014; Wilkins et al. 2016). However, results regarding the nature of underlying stellar populations are ambiguous due to possible contributions from nebular continuum and age-metallicity degeneracies (e.g. de Barros et al. 2014). These degeneracies can only

⋆ Based on observations obtained with *HST*/WFC3 program 14495 and the VLT programs 294.A-5018 and 294.A-5039.
† E-mail: d.sobral@lancaster.ac.uk

© 2017 The Authors

be overcome by direct spectroscopic observations that trace different states of the inter-stellar medium (ISM), but such observations have so far been relatively limited due to the faintness of sources.

Bright targets from wide-field ground based surveys (e.g. Bowler et al. 2014; Matthee et al. 2015; Hu et al. 2016; Santos et al. 2016; Shibuya et al. 2017a; Zheng et al. 2017) provide unique opportunities to obtain the first detailed and resolved studies of sources within the epoch of re-ionisation. These bright sources are particularly suitable for follow-up with ALMA (e.g. Venemans et al. 2012; Ouchi et al. 2013; Capak et al. 2015; Maiolino et al. 2015; Smit et al. 2017). While some sources seem to be relatively dust free (e.g. Ota et al. 2014; Schaerer et al. 2015), consistent with metal-poor local galaxies, others seem to already have significant amounts of dust even at $z > 7$ (e.g. Watson et al. 2015). Interestingly, the majority of sources is resolved in multiple components in the rest-frame UV (e.g. Sobral et al. 2015; Bowler et al. 2017a; Matthee et al. 2017c) and/or in rest-frame FIR cooling-lines (e.g. Maiolino et al. 2015; Carniani et al. 2017; Matthee et al. 2017a; Jones et al. 2017a).

High redshift galaxies appear to have ubiquitous high equivalent width nebular emission lines (e.g. Sobral et al. 2014; Smit et al. 2014, 2016; Mármol-Queraltó et al. 2016; Khostovan et al. 2016; Faisst et al. 2016). This may be linked to an elevated production efficiency of ionising photons per unit UV luminosity (Bouwens et al. 2016; Matthee et al. 2017b; Stark et al. 2017). Studies also find that the fraction of UV-selected Lyman-break galaxies with strong Lyα emission rises with redshift from at least $z \sim 3$ to $z \sim 6$ (e.g. Stark et al. 2010; Hayes et al. 2011; Schenker et al. 2012). Such trend may well continue into the epoch of re-ionisation, but the non zero neutral fraction beyond $z \sim 6$ makes Lyα fainter and hence harder to observe (see Schenker et al. 2012; Treu et al. 2013; Schenker et al. 2014; Pentericci et al. 2014). Recent results also highlight that high redshift galaxies have hard ionising spectra (see also Senchyna et al. 2017), revealed by UV emission lines such as CIII] and CIV (e.g. Stark et al. 2015). This is in line with results showing an increase in the ionisation parameter with redshift (Erb et al. 2010; Nakajima & Ouchi 2014; Khostovan et al. 2016).

Identifying the source(s) of such high ionisation conditions is a major challenge. Many mechanisms/physical processes have been proposed. These include binary stars, bursty star formation histories, active galactic nuclei (AGN), or a higher cut-off mass in the initial mass function (e.g. Eldridge & Stanway 2012; Gräfener & Vink 2015; Stanway et al. 2016; Sparre et al. 2017).

In this paper we focus on the COSMOS Redshift 7 Lyα emitter (hereafter CR7, $z = 6.604$, $L_{Ly\alpha}$=$10^{43.8}$ erg s^{-1}, $EW_{0,Ly\alpha} = 211$ Å; Sobral et al. 2015), a remarkably luminous source within the epoch of re-ionisation. CR7 reveals a potential narrow HeII1640Å emission line and no detection of any metal emission line at the current observational limit in the UV. As explained in Sobral et al. (2015), any 'normal' metallicity source would have been detected in CIV or CIII], indicating that the metallicity of CR7 should be very low (e.g. Hartwig et al. 2016). As the ionisation energy of HeII is 54.4 eV, the ionising source in CR7 must be very hot, with an expected effective temperature of $T \sim 10^5$K, hotter than normal stellar populations. Due to its unique properties, CR7 has been discussed in several studies, some focusing on one of the hypotheses discussed in Sobral et al. (2015) that it could harbour a direct collapse black hole (DCBH, e.g. Pallottini et al. 2015; Hartwig et al. 2016; Smith et al. 2016; Agarwal et al. 2016, 2017; Pacucci et al. 2017). However, as Dijkstra et al. (2016) shows, the DCBH interpretation has significant problems and realistically it cannot be favoured over e.g. PopIII-like (i.e. very low metallicity) stellar populations. Dijkstra et al. (2016) also argued that CR7's Lyα line is well explained by outflowing shell models, similarly to lower redshift Lyα emitters (e.g. Karman et al. 2017; Gronke 2017).

Other authors have studied and discussed CR7 by (re-)interpreting measurements provided by Sobral et al. (2015) and presenting novel results from e.g. de-convolving IRAC/*Spitzer* data (Agarwal et al. 2016; Bowler et al. 2017b). Such studies have reached similar observational results but often contradictory interpretations. For example, Bowler et al. (2017b) identifies the brightest UV clump in CR7 (clump A) as likely the brightest at 3.6 μm and interprets such brightness as potential [OIII] 5007 emission, using it to argue for a very low metallicity population with significant binary contribution, or a low metallicity AGN. Others (e.g. Agarwal et al. 2017; Pacucci et al. 2017) argue that those are the signatures of a "post-"DCBH. Bowler et al. (2017b) also shows that due to large systematics in Ultra-VISTA data, CR7's J magnitude has changed by +0.2 mag from the data used in Sobral et al. (2015), which makes the SED signature for HeII based on photometry much less convincing. Shibuya et al. (2017b) presented spectroscopic results of luminous Lyα emitters, and analysed X-SHOOTER data for CR7 to reach similar conclusions as Sobral et al. (2015) regarding Lyα, but finding a less-significant HeII line. More recently, Matthee et al. (2017a) detected [CII] in each of CR7's clumps with ALMA, with hints of a spectroscopically-backed multiple-major merger in CR7.

Several important questions remain unanswered regarding CR7, and these are some of the most important questions regarding the general population of galaxies at $z \sim 7$. What is (are) the ionising source(s) and what is (are) the metallicity(ies)? What constraints can we obtain on the major emission lines and on the continuum? Is the source variable?

In this paper, we obtain new *HST*/WFC3 resolved grism data, re-analyse and re-interpret previous spectroscopic data to further unveil the nature of CR7. In §2 we present the observations, data reduction and re-analysis of spectroscopic data. Results are presented in §3, addressing the differences in the 2D Lyα profile, the potential variability of the source, and constraining the fluxes from HeII and other UV emission lines from a combination of all data. We make predictions for the rest-frame UV and optical emission lines to be observed with JWST in §4, based on the best current observations and our CLOUDY modelling. We discuss results in §5 and present conclusions in §6. Throughout this paper, we use AB magnitudes, a Salpeter (Salpeter 1955) IMF and a ΛCDM cosmology with $H_0 = 70\,\mathrm{km\,s^{-1}\,Mpc^{-1}}$, $\Omega_M = 0.3$ and $\Omega_\Lambda = 0.7$.

2 OBSERVATIONS OF CR7

CR7 (Sobral et al. 2015) was identified as a luminous Lyα candidate by Matthee et al. (2015), while its UV counter-

part was independently found as a bright, but unreliable, $z \sim 6$ candidate Lyman-break galaxy (Bowler et al. 2012, 2014). CR7 was spectroscopically confirmed as a luminous Lyα emitter by Sobral et al. (2015) through the presence of a narrow, high EW Lyα line (FWHM= 266 km s^{-1}, EW$_0$ = 211 Å). Sobral et al. (2015) estimated that its luminosity was roughly double of what had been computed in Matthee et al. (2015), due to the Lyα line being detected at $\sim$ 50% transmission of the narrow-band filter used in Matthee et al. (2015). One of the reasons that made CR7 an unreliable $z \sim 6-7$ candidate Lyman-break galaxy (LBG) was the presence of an apparent J band excess of roughly $\sim 3\sigma$ based on UltraVISTA DR2 data (Sobral et al. 2015) and the strong Lyα contamination in the z band. CR7 was also identified as having a 3.6 μm excess, discussed as potential e.g. [OIII]5007 emission for the source as a whole in Matthee et al. (2015); see also Bowler et al. (2017b). The spectroscopic confirmation of CR7 as a Lyα emitter at $z = 6.6$ and the J band excess provided strong hints that an emission line should be contributing to the flux in the NIR. The shallow NIR spectra of CR7 showed only one emission line in the J band, interpreted as narrow HeII1640Å ($v_{\rm FWHM} = 130\,{\rm km\,s^{-1}}$), while no metal line was found. Such observations made CR7 relatively unique, not only because it became the most luminous Lyα emitter at high redshift, but also due to being a candidate for a very low metallicity star-burst ("PopIII-like"), a very low metallicity AGN and/or a candidate for a DCBH.

2.1 Imaging Observations and SFR properties from *HST* and ALMA

HST imaging reveals that CR7 consists of three "clumps" (Sobral et al. 2015; Bowler et al. 2017a); see Figure 1. We note that slit spectroscopic follow-up was targeted roughly at the peak of Lyα flux, and thus roughly at the position of clump A (see Figure 1), but without knowing that the source could be resolved in 3 UV clumps. Therefore, clumps B and C were not originally spectroscopically confirmed even though they are within the Lyα halo as observed with the narrow-band data and have a Lyman-break consistent with $z > 6$. Deep, high spatial and spectral resolution ALMA [CII] data have nonetheless allowed to spectroscopically confirm each of the UV clumps A, B and C as being part of the same system. Readers are referred to Matthee et al. (2017a) for a discussion on the spectroscopic confirmation of both clumps B and C and on the further dynamical and physical information inferred from the ALMA data.

Clump A, the brightest ($M_{UV} = -21.6 \pm 0.1$; Matthee et al. 2017a) and bluest, roughly coincides with the peak of Lyα emission and has a UV slope β (corrected for the contribution of Lyα to the F110W photometry) of $\beta = -2.3 \pm 0.4$ (measured within a 1″ diameter aperture; Matthee et al. 2017a). Clumps B and C are fainter ($M_{UV} = -19.8 \pm 0.2$ and $M_{UV} = -20.1 \pm 0.1$, respectively; Figure 1) and show $\beta = -1.0 \pm 1.0$ and -2.3 ± 0.8 in 0.4″ apertures. As the UV slopes are quite uncertain, they allow for large dust attenuations and hence uncertain SFRs. However, as shown in Matthee et al. (2017a), constraints on the IR continuum luminosity from very deep ALMA observations of CR7 can mitigate these uncertainties. In practice, as CR7 is undetected in dust continuum, it implies a relatively low

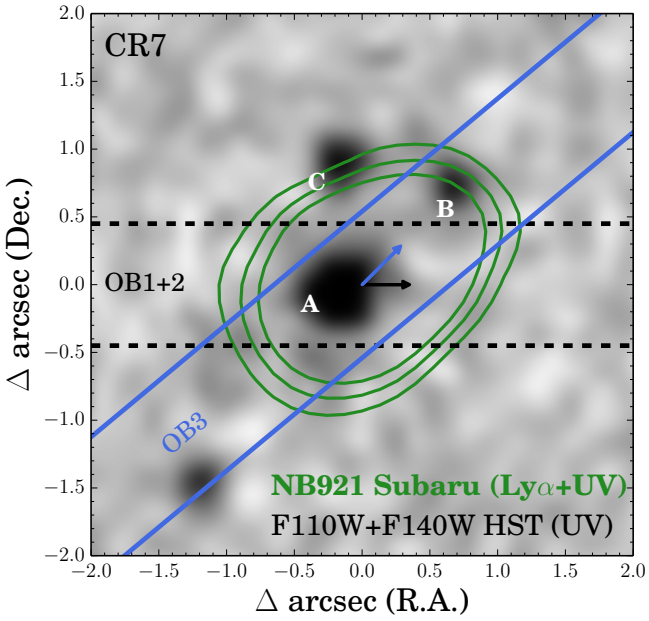


Figure 1. The *HST*/WFC3 image showing the rest-frame UV, and the NB921 ground-based Lyα contours of CR7 (Matthee et al. 2015; Sobral et al. 2015). We also show the approximate position, rotation and on-sky width (0.9″) of the X-SHOOTER slit used for the 3 OBs. For $z = 6.6$, 1″ corresponds to roughly 5.4 kpc. Note that although formally on the same location and with a PA angle of 0 deg, OB1 and OB2 yield different results, as OB1 was not well acquired by a few hundred miliarcsec. We also show two arrows pointing towards positive spatial locations in the reduced 2D spectra, i.e., positive offsets in the Y coordinate of the reduced 2D (see e.g. Figure 2). While OB1 and OB2 should sample more along component A of CR7 only (although it may still get some light from B towards the right; 'up' in the spectra spatial direction), OB3 runs from A to B. The UV component of clump C is not directly targeted, except for perhaps some of its light making it into OB3.

FIR luminosity of $L_{\rm IR}(T_d = 35\,{\rm K}) < 3.1 \times 10^{10}\,L_\odot$ and a dust mass $M_{\rm dust} < 8.1 \times 10^6\,M_\odot$ (3σ limits). Such limits imply a maximum dust obscured star formation rate of $< 5.4\,M_\odot\,{\rm yr^{-1}}$ for the full system. Overall, the combination of *HST* and ALMA observations reveal dust-corrected $SFR_{\rm UV+IR} = 28^{+2}_{-1}, 5^{+2}_{-1}, 7^{+1}_{-1}\,M_\odot\ {\rm yr^{-1}}$ (see Matthee et al. 2017a) for clumps A, B and C, respectively, for a Salpeter IMF (and a factor ≈ 1.8 lower for a Chabrier IMF). The SFR of the full CR7 system (A,B,C) is $45^{+2}_{-2}\,M_\odot\ {\rm yr^{-1}}$, taking into account the ALMA constraints for obscured SFR, and for a Salpeter IMF.

2.2 Re-analysis of X-SHOOTER observations of CR7

We re-analyse the X-SHOOTER data originally presented in Sobral et al. (2015). The NIR spectroscopic data in Sobral et al. (2015) were flux-calibrated using UltraVISTA J band photometry (which showed a strong J band excess), which was later shown to be significantly lower (see Bowler et al. 2017b). We investigate this large change in UltraVISTA J band data separately in Section 3.2.

The VLT/X-SHOOTER data were obtained over 3 dif-

ferent observing blocks (OBs; see Figure 1) of about 1 hour each, with two OBs obtained on 22 January 2015 and a final OB (a repeat of OB1, which we name OB3 in this paper, but that is formally called 'OB1' in the ESO archive) done on 15 February 2015. We reduce all OBs separately. All OBs used a 0.9″ slit in both the VIS and NIR arms; see Figure 1.

For the first two OBs a PA angle of 0 deg was used (see Figure 1), together with an acquisition source at 10:01:03.156 +01:48:47.885. Offsets of −77.266″ (R.A.) and −32.634″ (Dec.) were used to offset from the acquisition source to CR7. The acquisition for the first OB (OB1, 22 January 2015) was suspected to be relatively off-target due to an unreliable acquisition star centring (acquisition star was not centred in the slit), leading to an apparent lower Lyα flux and a spatially truncated and complex/double peaked Lyα profile, different from that found in the OB2 which was done with a good acquisition and with e.g. Keck/DEIMOS data (see Figure 2 and Sobral et al. 2015). When repeating OB1 and in order to avoid problems with acquisition, another acquisition source was used: 10:01:00.227, 01:48:42.992, applying an offset of −33.342″ (R.A.) and −27.742″ (Dec.) and this time with a PA angle of −39.76 deg, in order to better align the slit with the elongation of the Lyα 2D distribution obtained from the narrow-band imaging; see Figure 1.

We use the X-SHOOTER pipeline (v2.4.8; Modigliani et al. 2010), and follow the steps fully described in Matthee et al. (2017c), including flux calibration. We note that our new reduction results in a significantly improved wavelength calibration in the NIR arm when compared to Sobral et al. (2015), which we find to be off by $\sim -2-3$ Å in the NIR arm when compared to our improved reduction (due to the use of old arcs; see also Shibuya et al. 2017b, who find a similar result by using the most up-to-date pipeline). In the VIS arm we find no significant differences in the wavelength calibration when comparing to Sobral et al. (2015), but we now flux calibrate the data (using appropriate telluric stars) without relying on any narrow or broad band photometry, unlike Sobral et al. (2015). In Figure 2 we show the reduced 2D centred on Lyα for each individual OB (note that the positive spatial direction is indicated with an arrow in Figure 1). We also show the combined stack of the 3 OBs and when combining only the 2 final OBs. We present the results in Section 3.1.

Our reduced spectra show a spectral resolution (FWHM based on sky lines) of ≈ 1.2 Å at ≈ 9000 Å ($\approx 40\,\mathrm{km\,s^{-1}}$), corresponding to $R \sim 7500$ and ≈ 3.4 Å at $\approx 16{,}000$ Å ($\approx 60\,\mathrm{km\,s^{-1}}$), corresponding to $R \sim 4700$. In order to improve the signal-to-noise, we bin our 1D spectra to the resolution by using bins of 1.1 Å in the VIS and 3.4 Å in the NIR arm.

2.3 Re-analysis of SINFONI observations of CR7

We also re-reduced the SINFONI data. The final data-cube in Sobral et al. (2015) was produced with equal weights for all exposures by using the SINFONI pipeline to reduce all the OBs together. The data were then scaled in Sobral et al. (2015) by assuming the J magnitude from UltraVISTA and the flux implied for HeII from UltraVISTA. Finally, the stack was combined with X-SHOOTER data which had a systematic offset in wavelength by 3 Å, as stated in Section 2.2.

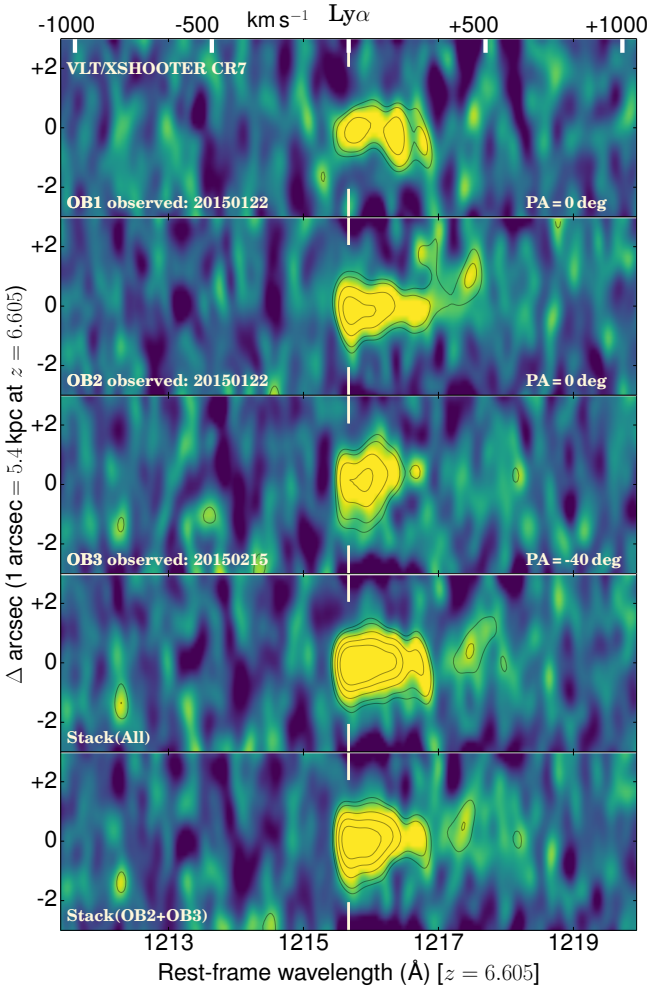


Figure 2. Our reduced and flux calibrated 2D X-SHOOTER spectra, zoomed-in at Lyα, in S/N space showing 1.5,2,3,4 and 5 σ contours. We find a tentative difference in the flux distribution between the 3 OBs, with this being caused by an incorrect target acquisition in OB1 (OB1 and OB2 were done consecutively on the same night but OB2 resulted from a better acquisition of the offset star), and particularly due to a different slit angle and offset star when comparing OB2 and OB3. Along the Lyα axis, expected from the NB, we find slightly more extended Lyα emission (as expected), but we also find a profile that is consistent with begin even narrower.

CR7 was observed with SINFONI in Mar-Apr 2015 (program 294.A-5039) with 6 different OBs of about 1 hour each. Four of those OBs were classed A (highest quality), one of them was classed B (seeing > 1″) and another one was classed C (bad quality, due to clouds). Here we neglect the one classed C.

We use the SINFONI pipeline v.2.5.2 and implement all the steps using ESOREX. We reduce each OB with the appropriate calibration files, done either on the same night or on the closest night possible. We reduce each OB individually, along with each standard/telluric star. In total, 5 different telluric stars were observed, 1 per OB/night of observations, and we reduce those observations in the same way as the science observations. In order to flux calibrate we use 2MASS JHK magnitudes of each star. We extract

the standard stars' spectra by obtaining the total counts per wavelength (normalised by exposure time) in the full detector, following the procedure in the pipeline, and we then re-extract them over the apertures used to extract the science spectra. This allows us to derive aperture corrections which vary per OB (due to seeing), which are typically ∼1.5 for 1.4″ extraction apertures, and ∼1.2 for 2″ aperture extractions.

We find that the absolute astrometry of the pipeline reduced data-cubes is not reliable, as each OB (which is done with the same offset star and with the same jitter pattern) results in shifts of several arcsec between each reduced data-cube. We attempt to extract spectra in the R.A. and Dec. positions of CR7 assuming the astrometry is correct but fail to detect any signal, with the stacked spectra resulting in much higher noise. Finally, we make the assumption that the data cubes are centred at the position of the first exposure which serves as reference for the stack of each OB, and extract 1D spectra per OB with apertures of 0.9″, 1.4″ and 2″ (using our aperture corrections). We estimate the noise per wavelength on each extracted spectra by randomly picking apertures within the wavelength slice and computing the standard deviation of the sum of the flux. Finally, we stack spectra from the different OBs by weighting them with the inverse of the variance/noise. Reduced SINFONI spectra have a resolution (FWHM, based on OH lines) of ~ 6.4 Å at $\sim 1.2\,\mu$m ($R \sim 1900$; $\sim 150\,\mathrm{km\,s^{-1}}$). When binned to the resolution, the spectra (1.4″ apertures, stacked) reach a 1σ flux limit of $\approx (2 \pm 1) \times 10^{-18}\,\mathrm{erg\,s^{-1}\,cm^{-2}\,\AA^{-1}}$, with the standard deviation reflecting noisier regions affected by OH/sky lines.

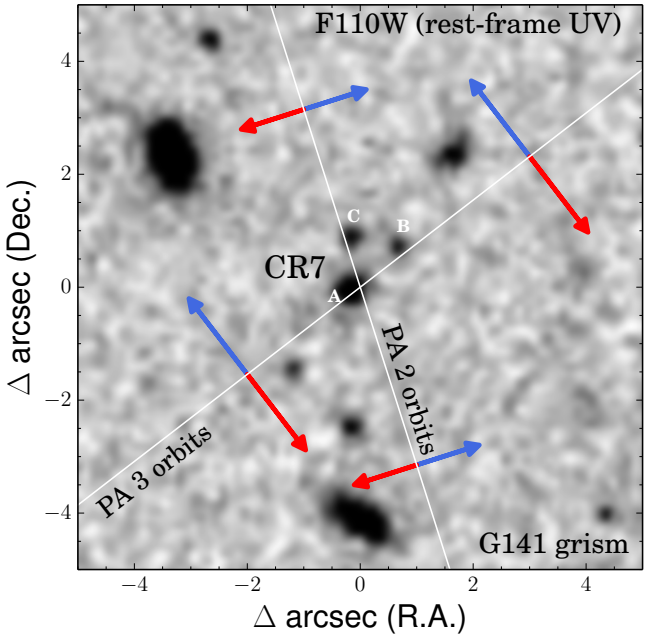


Figure 3. HST/WFC3 F110W ($Y + J$) image centred on CR7 and the immediate surroundings for our G141 grism observations. We indicate the PA angles used for each of the 2 visits done: one observing for 2 orbits and the final one observing for 3 orbits. We also indicate the dispersion direction and the direction in which bluer/redder light gets dispersed once the grism is used to take observations. Our observations allow us to avoid contamination from nearby sources and obtain spectra for each of the components A, B and C for CR7.

2.4 WFC3/*HST* grism Observations

We observed CR7 with the WFC3 grism with GO program 14495 (PI: Sobral). Observations were conducted over a total of 5 orbits: 2 orbits during 21 Jan 2017 and 3 further orbits conducted during 17 Mar 2017. We used two different PA angles (252.37 deg and 322.37 deg; see Figure 3), each calculated to avoid significant contamination by nearby bright sources and in order to investigate the spectra of A, B and C separately.

For each orbit, we obtained an image with the F140W filter, two grism observations (dithered) with the G141 grating (central wavelength 13886.72 Å), and another image after the second grism observation. These allow us to correctly identify the sources and to clearly locate clumps A, B and C within CR7. The F140W images were obtained at the start and end of each orbit with the aim to minimize the impact of variable sky background on the grism exposure (due to the bright Earth limb and the He 1.083 μm line emission from the upper atmosphere; see Brammer et al. 2014). A four-point dithering pattern was used to improve the sampling of the point-spread function and to overcome cosmetic defects of the detector.

We obtain imaging exposures of ~ 0.25 ks and grism exposures of ~ 1.10 ks. Our total exposure grism time with G141 is 11.0 ks. For a full description of the calibration of the WFC3/G141 grism, see e.g. Kuntschner et al. (2010).

2.4.1 *Data reduction and extraction*

We reduce the data following Brammer et al. (2012). The grism data were reduced using the grism reduction pipeline developed by the 3D-*HST* team (e.g. Brammer et al. 2012; Momcheva et al. 2016). The main reduction steps are fully explained in Momcheva et al. (2016). In summary, the flat-fielded and global background-subtracted grism images are interlaced to produce 2D spectra for each of clumps A, B and C, independently. We also identify any potential contamination from faint and/or nearby sources and subtract it when we extract the 1D spectra. Our reduced data show a resolution of $R \sim 100$ (FHWM 150 Å) at $\lambda \sim 1.2\,\mu$m, and thus a resolution of ~ 20 Å at ~ 1600 Å rest-frame for CR7 in Lyα ($z = 6.605$).

We extract the spectra of the 3 major components of CR7 from their central positions by using the rest-frame UV continuum images obtained with *HST*. We see clear continuum in the 2D for clump A (the brightest) and weak continuum from B. We find that apart from some minor contamination at observed $\lambda \sim 15500 - 15700$ Å, the spectrum of the 3 clumps of CR7 is not contaminated by any other nearby sources, as expected from our observing planning (Figure 3). We thus estimate the noise on the CR7 spectrum by extracting spectra in a range of spatial locations (per clump) with similarly low contamination. We use the standard deviation per wavelength as the estimate of our $1\,\sigma$ error and we use these to quantify the signal to noise and to evaluate the significance of both the continuum and

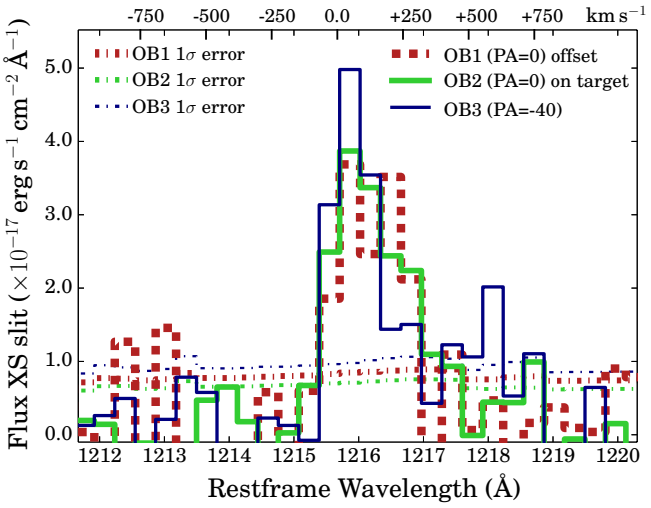


Figure 4. The extracted 1D spectra from X-SHOOTER at the position of Lyα showing results from different OBs which trace different spatial scales and different angles for CR7 (see Figure 1). We show spectra binned by 75 km s^{-1} (roughly double the resolution). We find that OB3, that traces along the Lyα major axis, connecting A to B, shows the highest flux peak and the narrowest Lyα profile, with a FWHM $\sim$ 200 km s^{-1}. OB1, which was off-target and with a PA angle of 0 deg shows a broader Lyα profile, tentatively double peaked, which could point towards complicated dynamics. OB2, obtained with the same angle but closer to the peak of Lyα emission also shows a broader Lyα profile than OB3. Interestingly, OB3 may also show a higher redshift component at around 500-600 km s^1 from the peak of Lyα, but this is found at relatively low significance.

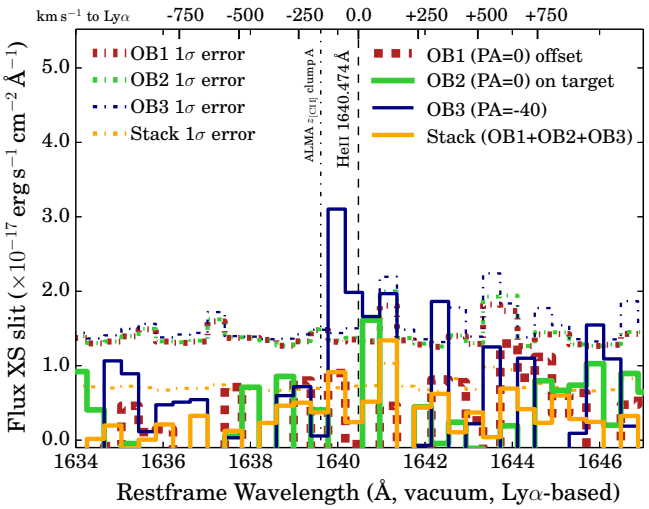


Figure 5. The extracted 1D spectra from our X-SHOOTER re-analysis and the multiple OBs and full stack at the expected location of HeII. Peaks in the 1 σ noise indicate the location of OH lines. We find no significant HeII detection for CR7 in the spatial locations covered by OB1 and OB2, and also no significant detection in the stack of the 3 OBs. However, we find a tentative detection (which dominates the signal in Sobral et al. 2015), consistent with a narrow HeII line in CR7 in OB3. We show the expected location of the HeII line in the case of no velocity shift from Lyα and also where we would expect to detect based on [CII]-ALMA emission from clump A. We find that the potential HeII signal is consistent with a relatively small velocity offset from Lyα of $\sim$ 100 km s^{-1} and would imply a similar redshift to the one obtained with [CII].

the detection of any emission lines. Our un-binned spectra of each of the 3 components of CR7 show a noise level of $\sim (3-19) \times 10^{-20}$ erg s^{-1} cm^{-2} Å^{-1}.

3 RESULTS

Here we present the results from new spectroscopic observations with *HST*, together with a re-analysis of both X-SHOOTER and SINFONI data from the VLT. We first present the results from each data-set and interpret them together at the end of the Section.

3.1 Results from ground spectroscopy

3.1.1 Spatially resolved Lyα in X-SHOOTER

In Figure 2 we show the 2D spectra for our re-analysis of the X-SHOOTER data, in a signal-to-noise scale, focusing on Lyα. We find potential variations in the Lyα profile, indicating that we are probing different spatial regions within the source. This is likely due to the bad acquisition for OB1 (in comparison to OB2) and due to a different acquisition star and PA angle for OB3. While of relatively low significance, OB3 suggests a slightly redshifted component of Lyα in the rough direction of clump B (see also Figures 1). As can be seen in more detail in Figure 4, OB3 also reveals an even narrower Lyα profile ($\sim$ 200 km s^{-1}) than OB2 ($\sim$ 340 km s^{-1}), hinting that the Lyα FWHM may be even narrower along the major axis of Lyα (running from A to B), but both OB2 and OB3 show the same/similar blue cut-off. A potential explanation for this may be actual dynamics within the system, as the major axis of Lyα emission, that roughly connects A to B may be the axis of some potential merger activity (Matthee et al. 2017a). Matthee et al. (2017a) also finds that the perpendicular axis shows the largest velocity shift (Figure 4), from the most blueshift towards C to the highest redshift towards the opposite direction, and with a total velocity shift of $\sim$ 300 km s^{-1}, similar to the Lyα FWHM in OB2. It may well be that Lyα itself is tracing such complex dynamics, or that we are seeing more complex radiation transfer effects or different HI column densities; observations with e.g. MUSE and further modelling can further clarify this.

3.1.2 HeII in X-SHOOTER: reliability and flux constraints

We show our re-analysis of X-SHOOTER data, split by OB, in Figure 5, where we present the extracted 1D spectra, binned to a resolution (FWHM) of 75 km s^{-1} at the expected rest-frame wavelength of HeII. We also present the 2Ds, per OB, showing Lyα and HeII for an easy comparison in Figure 6, where we show the 2D spectra of the expected location of HeII based on the Lyα redshift. Our re-analysis is able to recover the HeII signal claimed in Sobral et al. (2015), but clearly shows that the signal is coming essentially all from

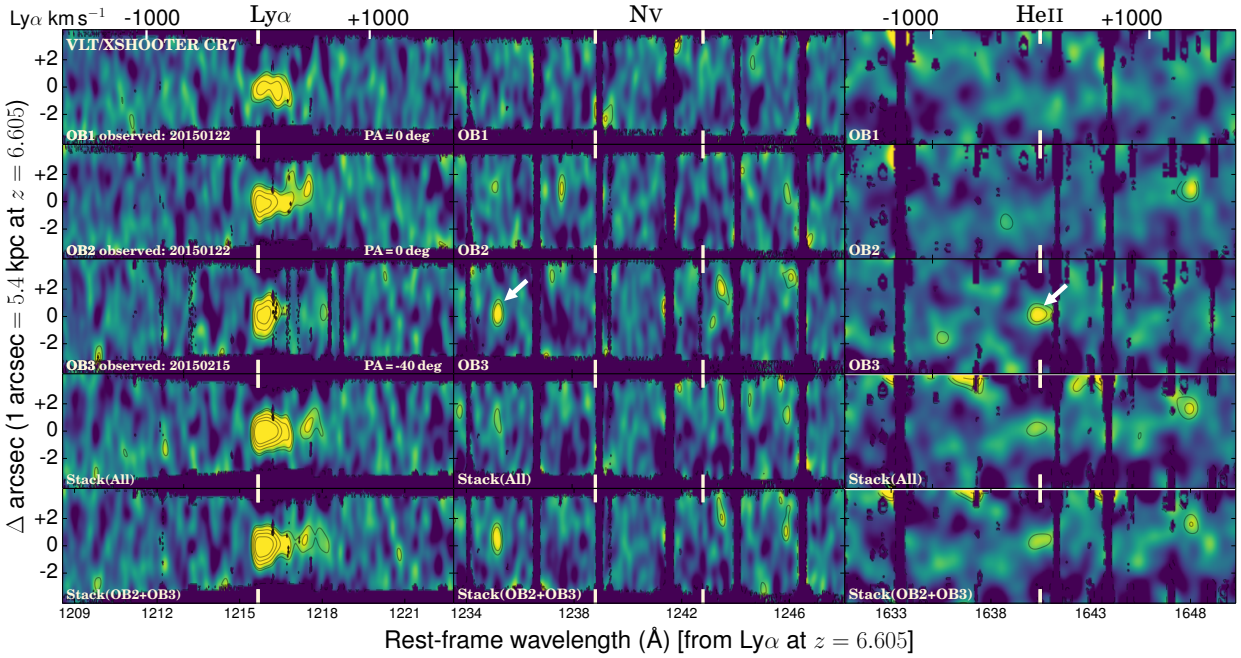


Figure 6. Our final reduced and flux calibrated 2D X-SHOOTER spectra, zoomed-in at the expected positions of Lyα, NV and HeII. We show spatial contours of 1.5,2,3,4 and 5 σ. In order to highlight the location of sky lines and noisy regions in the 2D, we identify, in each spectral window, pixels that deviate in more than 20% from the the median local noise and set such regions below the cut-off (they are shown in dark). We find a tentative difference in the Lyα profile and in the Lyα fluxes measured between the 3 OBs, with this likely being caused by an incorrect target acquisition in OB1 (OB1 and OB2 were done consecutively on the same night but OB2 resulted from a better acquisition of the offset star), and a different slit angle and offset star when comparing OB2 and OB3. We see that the detection of HeII is only seen for OB3 at a $\approx 2.6\,\sigma$ level, also showing the negatives up and down and in the same spatial location as Lyα. Furthermore, in OB3 we also find a tentative emission line blue-shifted by $\sim 800-900\,\mathrm{km\,s^{-1}}$ to the expected wavelength of NV. Such potential line is not significant when stacking the full data, but can also be seen in the stack of OBs 2 and 3.

OB3 (see Figures 5 and 6), which was aligned with the major axis of the Lyα extent, and that shows the highest Lyα flux peak (Figure 4). Based on OB3 only, we find a tentative HeII detection at the $\approx 2.5-2.7\,\sigma$ level. We can also see the negatives up and down from the offsets along the slit (Figure 6), in the same locations as for e.g. the Lyα line, which propagate to the final stack. These are typically taken as clear indications that an emission line is real (as opposed to e.g. a line which only shows a negative up or down or no negatives). This potential emission line seen in OB3 has a flux of $(1.8\pm0.7)\times10^{-17}\,\mathrm{erg\,s^{-1}}$ and a FWHM $\sim 170-200\,\mathrm{km\,s^{-1}}$ (similar to the Lyα FWHM in OB3). The lower flux we find compared to Sobral et al. (2015) is due to the different flux calibration which in Sobral et al. (2015) was based on Ultra-VISTA J band. The potential HeII signal from OB3 is consistent with a redshift of $z = 6.603\pm0.001$, and thus implies a relatively small velocity offset from Lyα of $\sim 100\pm50\,\mathrm{km\,s^{-1}}$ being closer in velocity to the systemic redshift of clump A ($z = 6.601\pm0.001$; see Figure 5), than to the slightly lower redshifts measured for the other components in the CR7 system ($z = 6.593-6.600$; Matthee et al. 2017a). This would argue for the line being more likely associated with A, originating in another sub-component of the system (slightly redshifted from A), and/or being evidence for variability or for it to be spurious. Interestingly, by further splitting OB3 in multiple sets of exposures, we can still see emission consistent with the final signal, spread over the majority of the exposures, and also revealing negatives in most sets of exposures. This means the signal is not a cosmic ray or an artefact. Nevertheless, given the low signal-to-noise from just one OB there is still the chance that some significant OH variability during the observations could have at least contributed to boosting the signal somewhat, although the errors take OH lines into account.

When we analyse OB1 and OB2 separately (see Figure 5) we find no evidence of the presence of HeII, with a flux upper limit ($3\,\sigma$) of $< 2.4\times10^{-17}\,\mathrm{erg\,s^{-1}}$ for a $200\,\mathrm{km\,s^{-1}}$ FWHM line at $z = 6.603-6.605$.

Due to the improved wavelength calibration we can better identify flux coming from sky line residuals and we also mask them in Figure 6. Overall, we find that with our direct flux calibration and combining spectra based on the inverse of the noise, the combined HeII signal of the full stack of 3 OBs is significant at only $\sim 1.5-1.9\,\sigma$. Thus, based on the full stack we find similar results as Shibuya et al. (2017b). Similarly to Shibuya et al. (2017b), we can see the potential negatives up and down which should be signatures of a real line. However, we clearly show that all the signal comes from OB3, where the line is tentatively detected at $\sim 2.5-2.7\,\sigma$, as discussed (Figure 6).

3.1.3 Searching for other lines in X-SHOOTER

We conduct an investigation of the full X-SHOOTER spectra, both on the full stack and also per OB, apart from Lyα and HeII. We search for UV rest-frame lines with FWHMs

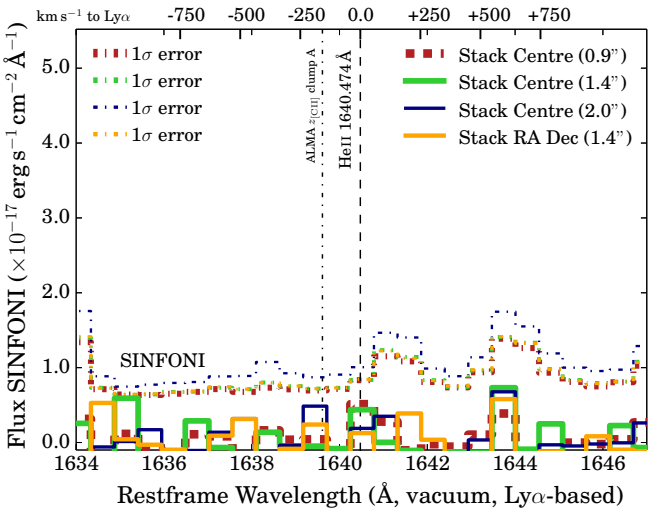


Figure 7. The extracted 1D from SINFONI at the expected location of HeII for the different stacks attempted for CR7. The stacks show extractions obtained on the centre of the detector with different extraction apertures (using the appropriate aperture corrections based on the standard stars available) and also based on the R.A./Dec. positions assuming the astrometry is accurate. We conservatively estimate the noise with randomly placed apertures per wavelength slice; these also show the locations of OH lines as peaks in the noise. In our stacks or individual OBs we find no significant detection of HeII or any other rest-frame UV line, although we note the caveats of the spatial location and any potential variability.

from 150 to 1500 km s^{-1} with redshifts from $z = 6.58$ to $z = 6.606$. We do not detect any line above $3\,\sigma$, but find a potential emission line just below the $3\,\sigma$ level ($\sim 2.5-2.9\,\sigma$) in OB3. We find it in the VIS arm (showing the negatives from offsetting along the slit; see Figure 6) spatially coincident with Lyα. For $z = 6.60$ the potential emission line (S/N$\sim$ 3) is relatively close to the expected rest-frame wavelength of the NV doublet (see Figure 6), but would imply a redshift of $z = 6.583 \pm 0.001$ for it to be 1238.8 Å (see e.g. Tilvi et al. 2016; Hu et al. 2017; Laporte et al. 2017, for NV detections in other sources at $z \sim 7$). It is possible that such source could be linked with a blue-shifted [CII] component seen in the ALMA data which is spatially coincident with clump C, implying an AGN nature for such source (or an AGN driven-outflow). This would mean that the potential NV line would not be linked with clump A, for which [CII] provides $z = 6.601$, but potentially clump C. If the potential NV line is real, it would be blue-shifted from the potential HeII line by $\sim 800 - 900$ km s^{-1}. Regardless of the association, it would also imply a very high NV/HeII ratio (> 0.5) only possible for very high ionisation parameters ($\log U \sim -1$) and low density gas being ionised by an AGN, found in high redshift radio galaxies (e.g. Matsuoka et al. 2009).

3.1.4 The nature of CR7 with SINFONI

One can further explore the reliability of HeII and its potential variability and spatial location by exploring the SINFONI data. The first observations were conducted 1 month after the X-SHOOTER OB3, and span a full month. In Figure 7 we show the 1D stacks. We show these for different extraction apertures and note that we assume the source is in the centre of the 3D stacked cube, per OB (see Section 2.3). We visually search for potential emission in 2D by binning the data spectrally based on the HeII signal in X-SHOOTER's OB3, and find potential signal from HeII in three of the OBs, consistent with those found in Sobral et al. (2015) by using SINFONI data only. However, by measuring the noise on such wavelength slices (with apertures of $\sim 1''$) we find that such signal on its own is always of low significance $< 1.5\,\sigma$, mostly due to the presence of the nearby sky-line and SINFONI's lower resolution. Nevertheless, we still extract 1D spectra based on such positions, and also compare the results.

By obtaining spectral extractions at the centre of each 3D stack we find no evidence for any significant emission line for rest-frame wavelengths of $\sim$ 1450 − 1770 Å (see e.g. Figure 7). This allows us to place a $3\,\sigma$ limit of $< 2 \times 10^{-17}$ erg s^{-1} cm^{-2} for HeII assuming a FWHM of 200 km s^{-1} and an aperture of $1.4''$. We cannot exclude the possibility that any signal is spatially spread in different ways and that our stacking leads to spreading it spatially in a way that becomes undetectable. We also note that the limit obtained with SINFONI is still formally consistent with the X-SHOOTER detection in OB3 ($1.8 \pm 0.7 \times 10^{-17}$ erg s^{-1} cm^{-2}), and thus it cannot exclude it easily at a $3\,\sigma$ level, and also does not exclude the detection even at a 2σ level based on the flux errors from X-SHOOTER. However, our SINFONI results certainly imply that the flux, if non-variable (and not spatially spread due to the data-reduction/stacking), should be at least towards the lower limit measured with X-SHOOTER, and thus closer to $\sim 1 \times 10^{-17}$ erg s^{-1}. This would imply an observed HeII/Lyα ratio of $\sim$ 0.06. As no convincing detection (based on the noise) is made in either of the SINFONI OBs, we are not able to comment on potential variability. Deeper data are therefore required to further test both the reliability and the potential variability of HeII.

3.2 Variability: UltraVISTA

We combine data from different epochs/data-releases of UltraVISTA (McCracken et al. 2012), attempting to constrain the potential variability of CR7. We find a large (in magnitude), 0.2-0.5 mag variation in the J band magnitude of CR7 from the UltraVISTA survey from DR2 to DR3 (see also Bowler et al. 2017b), while the magnitude apparently stayed constant from DR1 to DR2 (see Appendix B). We note, nonetheless, that from DR2 to DR3 no more exposures were obtained for the sky location of CR7, and thus the difference seems to be due to potential (strong) systematics on the data reduction by UltraVISTA. While 0.5 mag (becoming fainter) is quite a large change, and dramatically affects the interpretation of a high EW emission line in the J band (which was taken as a strong prior in Sobral et al. 2015), we find that, perhaps surprisingly, many other sources with a similar magnitude (see Figure B1) changed by this amount in the location of CR7, which imply magnitude errors on the UltraVISTA higher than the ones formally estimated in the catalogues. We therefore interpret the change not as intrinsic variability, but due to variations from the UltraVISTA

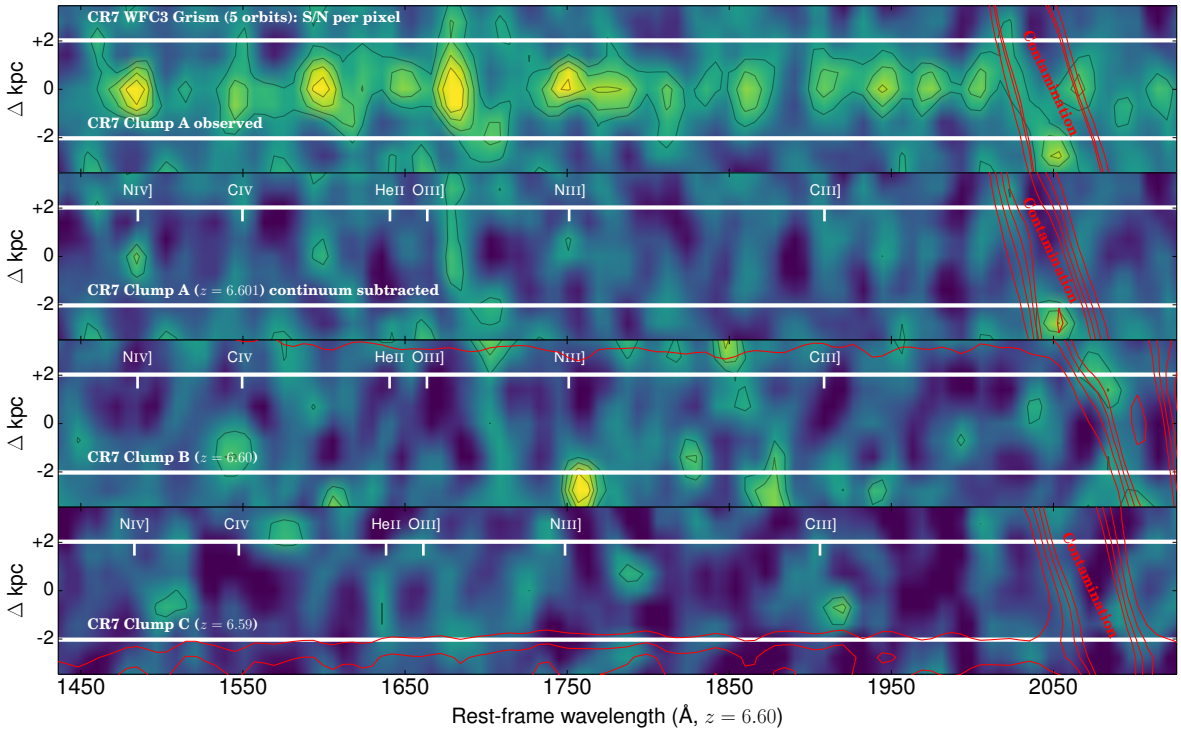


Figure 8. The final *HST*/WFC3 Grism 2D reduced spectra, smoothed by 1 spatial and spectral pixels, for each of the three UV clumps in CR7: A, B and C (see Figure 1). All 2D here are shown in S/N space (contours: 2, 3, 4, 5 σ), with the noise estimated away form the location where each clump is found. For A, we show both the observed spectra (top), which shows significant continuum detection and the continuum subtracted 2D spectra. For B we show only the continuum subtracted spectra. For C we do not detect any continuum and thus we do not subtract it. We show locations which were contaminated by nearby sources (contamination was subtracted but can still result in residuals). We also show the expected location of rest-frame UV lines using redshifts obtained with ALMA-[CII] (Matthee et al. 2017a) close to the position of each clump and also an indicative "slit" of 0.7″ that would contain close to 100% of the flux of each clump. We note that our 1D extraction is based on the 2D image of *HST* of each clump. Apart from detecting continuum, no clear emission line $> 3\,\sigma$ is found for any of the three clumps, and only tentative/low S/N detections are possible with the current data.

data reduction and source extraction. This also means that we cannot exclude a variability of CR7 below < 0.5 mag, although we can exclude a strong variability of > 0.5 mag.

3.3 *HST* Grism observations: continuum results

The spectrum of CR7 is extracted for its multiple UV components A, B and C detected with *HST* (see e.g. Figure 1). Figure 8 shows the 2D extractions per clump. We start by investigating the properties of the continuum and compare those with broad-band photometry. We use the extracted spectra but also bin the extracted spectra to resolutions of up to 8000 km s^{-1} for a high S/N of the continuum; see Figure 9. We measure M_{UV} (at rest-frame 1500 Å) by integrating the flux between rest-frame 1450 Å and 1550 Å, and we also fit a power law of the form λ^{β}. All measurements are conducted per UV clump. We find that our extraction of clump A yields $\beta = -2.4 \pm 0.4$ and $M_{UV} = -21.7 \pm 0.3$ (see Figure 9), and thus consistent with the photometric properties of the clump, estimated as $\beta = 2.3 \pm 0.4$ and $M_{UV} = -21.6 \pm 0.1$ (see e.g. Matthee et al. 2017a). This shows we are able to recover the continuum properties of clump A, and that at least these continuum properties show no significant evidence for variability (< 0.3 dex for clump A) within the errors. Note that previous photometric data were taken in 2012, and thus five years before the grism spectra (see Sobral et al. 2015). Our measurements are also independent of any emission-line contamination, which we can mask, and are not affected by e.g. strong Lyα emission. For clump B we find $\beta = -2.0 \pm 1.0$ and $M_{UV} = -20.7^{+0.3}_{-0.6}$, which compares with values of $\beta = -1.0 \pm 1.0$ and $M_{UV} = -19.6 \pm 0.7$ from photometry (see e.g. Matthee et al. 2017a). Note that, as shown in Figure 9, the continuum detection in clump B is of significantly lower S/N than that of clump A, and thus the UV properties derived are much more uncertain. As a consequence, we are also unable to place strong constraints on the variability of B. For clump C we do not make any significant continuum detection, but our spectra are consistent with $\beta \sim -2.8 \pm 1.0$ and $M_{UV} = -20 \pm 1$. We note that our detection of continuum in B and non-detection of C is unexpected given that previous UV photometry implied clump C was slightly brighter than B (e.g. Bowler et al. 2017b; Matthee et al. 2017a). This could mean that the relative brightness of clumps B and C could be varying.

Overall, from our grism spectroscopy, we find that clump A is $\sim 2-3$ times brighter in UV continuum than clumps B and C, and that, within the (large) errors, their β slopes are consistent with each other. We find tentative indications that clump *B* is redder than *A*, similarly to results from photometry, but our current errors do not allow for any strong conclusions to be made. Finally, we find tentative evidence for variability in clump C, having become

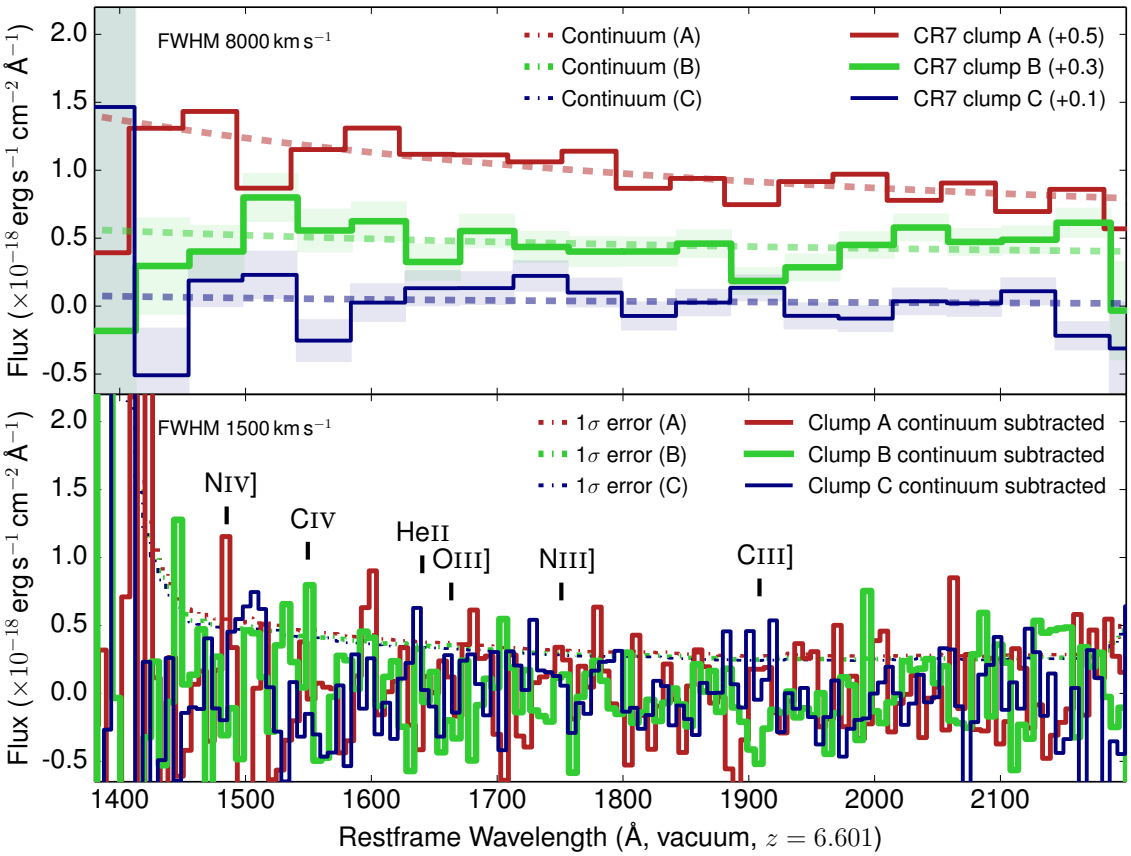


Figure 9. *HST*/WFC3 grism 1D spectra of the three different clumps of CR7 extracted based on the UV detections of each clump in the pre- and post-images of the grism observations. *Top:* Clump A is significantly detected in the UV continuum and is well fitted with a $\beta = -2.4 \pm 0.4$ and $M_{UV} = -21.7 \pm 0.3$. Clump B is also detected in the rest-frame continuum but at a much lower significance, while clump C is not detected in the continuum. Previous photometry (e.g. Bowler et al. 2017b; Matthee et al. 2017a) implies C should be brighter than B, and thus our results suggest that C may be variable. *Bottom:* After continuum subtracting the spectra of each clump we find no significant detection above $3\,\sigma$ of any rest-frame UV line. There are only weak/tentative detections ($\sim 2\,\sigma$) of NIV] in clump A and HeII in clump C (which would indicate $z = 6.58 \pm 0.01$ for that source, consistent with the blue-shifted component observed with ALMA towards the location of clump C). The resolved spectra also show that any potential HeII emission would have to likely come from or near clump C and not clump A. We assign relatively strong limits to all observed rest-frame UV lines, which we use to further interpret CR7.

fainter in our grism observations than expected from previous photometry. Observations with *HST*/WFC3 program 14596 (PI: Fan) will be able to further clarify/confirm our tentative indications.

3.4 Grism observations: emission-line results

Figure 8 presents our 2D spectra of each of the three clumps in CR7. For clump A we show both the observed (continuum-dominated) spectrum, along with the continuum subtracted, while for clump B we show the continuum subtracted spectrum only and for C we show the observed spectrum as we make no significant continuum detection (if anything we find a systematic negative signal). In Figure 9 we present the extracted 1D spectra of each clump.

By using the best continuum fits shown in Figure 9, we then continuum subtract the spectrum of each clump. We show the results in the bottom panel of Figure 9, now in the best resolution possible with the grism data, and in order to look for any emission or absorption lines. We find no clear rest-frame UV emission or absorption line above a $3\,\sigma$ level in any of the three clumps. Nonetheless, there are possible/tentative detections which are just above $\sim 2\,\sigma$: NIV] for the extraction of clump A ($z = 6.60 \pm 0.01$) and a potential weak detection of HeII for clump C (which would imply $z = 6.58 \pm 0.01$). Note that while NIV] for clump A is consistent with the systemic redshift now obtained for clump A with ALMA (Matthee et al. 2017a), the potential HeII detection towards C would be consistent with a redshift of $z = 6.58 - 6.59$. This could be related with the blue-shifted [CII] component found with ALMA towards C and also the potential NV (which would imply $z = 6.583 \pm 0.001$) detection also towards that spatial location in the system.

In order to better quantify the significance of all rest-frame UV lines, we measure all lines with GRIZLI[1]/Emcee (MCMC), by fitting simultaneously to all of the exposure level 2D spectra. We obtain the 2.5, 16, 50, 84 and 97.5 percentiles of the Emcee chain, and show the results in Table 1. Our results show that there are no clear ($> 3\,\sigma$) emission

[1] https://github.com/gbrammer/grizli/

Table 1. Results from the MCMC chain to constrain the line fluxes of each clump within CR7 for our *HST/WFC3* grism data (A, B and C) after subtracting the UV continuum per clump. All fluxes are in $10^{-18}\,\mathrm{erg\,s^{-1}\,cm^{-2}}$. We find no significant detection above $3\,\sigma$ of any UV line within any of the clumps. However, we find potential/weak detections of NIV] in clump A and HeII in clump C, both at just over $2\,\sigma$.

Emission Clump A	2.5% -2σ	16% -1σ	50% central	84% $+1\sigma$	97.5% $+2\sigma$
NIV] 1485	0.21	7.66	14.78	20.94	26.69
CIV 1549.5	-7.45	-2.23	3.13	8.70	15.07
HeII 1640.5	-13.60	-8.70	-3.66	1.48	5.46
OIII] 1663.5	-6.36	-2.27	2.33	7.11	11.22
NIII] 1751	-2.54	1.26	5.11	9.00	13.37
CIII] 1908.5	-5.45	-2.36	1.22	4.76	7.49
Clump B	-2σ	-1σ	central	$+1\sigma$	$+2\sigma$
NIV] 1485	-16.04	-11.06	-5.16	0.67	6.50
CIV 1549.5	-3.72	0.60	5.00	9.93	15.20
HeII 1640.5	-10.28	-6.35	-2.07	1.87	5.99
OIII] 1663.5	-14.24	-10.49	-6.08	-2.11	2.22
NIII] 1751	-9.27	-5.67	-2.04	1.42	4.33
CIII] 1908.5	-15.26	-12.33	-9.18	-6.14	-3.02
Clump C	-2σ	-1σ	central	$+1\sigma$	$+2\sigma$
NIV] 1485	-7.29	-1.88	4.52	10.06	15.44
CIV 1549.5	-10.57	-6.43	-2.34	2.24	6.72
HeII 1640.5	1.83	5.70	9.60	13.66	17.12
OIII] 1663.5	-8.08	-3.87	0.23	4.45	8.01
NIII] 1751	-4.19	-0.92	2.42	5.58	8.62
CIII] 1908.5	-1.93	0.98	4.01	7.09	9.83

line detection in either of the clumps (but note that there is a potential signature of CIII] in absorption for clump B, close to $\sim 3\,\sigma$). We also obtain very strong constraints on HeII from clumps A and B, showing no detections and a 97.5% probability of the HeII flux in each of those clumps being $< 6 \times 10^{-18}\,\mathrm{erg\,s^{-1}\,cm^{-2}}$, which compares with the X-SHOOTER potential detection of HeII towards B/C of $(18 \pm 7) \times 10^{-18}\,\mathrm{erg\,s^{-1}\,cm^{-2}}$. This strongly implies that any HeII signal in X-SHOOTER is not coming from the UV components of either A or B, as otherwise it should have been detected at a $\sim 4.5\,\sigma$ level. Interestingly, for clump C there is a potential signal from HeII, with only $< 2.5\%$ of realisations resulting in a flux lower than $< 1.8 \times 10^{-18}\,\mathrm{erg\,s^{-1}\,cm^{-2}}$ (see Table 1). For C, we find that 97.5% of realisations result in a HeII flux of up to $17.1 \times 10^{-18}\,\mathrm{erg\,s^{-1}\,cm^{-2}}$, with a central value of $(10 \pm 4) \times 10^{-18}\,\mathrm{erg\,s^{-1}\,cm^{-2}}$, which compares with the X-SHOOTER signal of $(18 \pm 7) \times 10^{-18}\,\mathrm{erg\,s^{-1}\,cm^{-2}}$. However, and even though the WFC3 grism resolution is relatively poor, we find that the tentative HeII flux would be blue-shifted ($z = 6.58 \pm 0.01$) in respect to what was found with X-SHOOTER ($z = 6.603 \pm 0.001$), and thus more consistent with the redshift derived for clump C with ALMA (Matthee et al. 2017a).

3.5 Summary of all observations

We have analysed CR7 as a whole with three different instruments and also by obtaining spectra for each of the three clumps. We find that despite a large change in the apparent J magnitude of CR7, current photometric and spectroscopic data are consistent with no variability both for the full system and also for each individual clumps at a level of $< 0.3 - 0.5$ mag, although there is tentative evidence for clump C to be variable. Our re-analysis of the X-SHOOTER data reveals clear differences in the spatial properties of Lyα and also identifies the tentative HeII signal presented in Sobral et al. (2015) as coming from the only X-SHOOTER OB which was aligned with the Lyα major axis, where the Lyα profile is the narrowest. Interestingly, apart from recovering HeII (although at a low significance), and revising its flux by measuring it independently of UltraVISTA J band data, we also identify a potential emission line which may correspond to NV at $z = 6.583 \pm 0.001$. Such finding may provide hints that the blue-shifted component towards clump C (found with ALMA; Matthee et al. 2017a) may harbour an AGN, but the significance of NV is too low for this to be claimed robustly: further observations are required. Furthermore, our re-analysis of SINFONI is able to recover a qualitatively similar signal to that of Sobral et al. (2015), but our re-analysis of the noise level/properties shows that there is no significant HeII detection from CR7 in the SINFONI data-set – the reader is referred to Section 3.1.4 for the caveats with extraction, particularly due to the resolved nature of the system. Finally, by exploring much deeper and resolved spectroscopic observations (albeit with a strong loss in resolution) with *HST*, we are able to study each clump within CR7 in detail, by extracting their spectra based on their UV extents/locations. We detect the continuum of clump A significantly, and weakly in clump B. We fail to detect any UV line in any of the clumps above $3\,\sigma$, but we find a tentative detection of NIV] in clump A. We argue that the grism data provide strong evidence against HeII coming from clump A or B. Interestingly, the data are consistent with HeII emission at the level found with X-SHOOTER for clump C, where there may be some HeII emission at the level of $(10 \pm 4) \times 10^{-18}\,\mathrm{erg\,s^{-1}\,cm^{-2}}$, which compares with the X-SHOOTER signal (non-slit corrected) of $(18 \pm 7) \times 10^{-18}\,\mathrm{erg\,s^{-1}\,cm^{-2}}$. Our results thus clearly show that HeII is significantly weak in clump A, with the $2\,\sigma$ upper limit in clump A implying $< 5.5 \times 10^{-18}\,\mathrm{erg\,s^{-1}\,cm^{-2}}$, and thus a HeII/Ly$\alpha$ ratio < 0.06 for clump A, making A significantly less likely to harbour an AGN. However, the potential presence of NIV] in A is interesting (see discussion of a potential NIV] detection in a lensed Lyα emitter at high-z and potential implications, e.g. McGreer et al. 2017), as it would indicate a relatively hard ionising spectra.

4 CLOUDY MODELLING AND PREDICTIONS FOR JWST OBSERVATIONS OF CR7

Here we explore the best constraints on a variety of lines (see Tables 2 and 4) to infer the possible physical properties of CR7, exploring its uniqueness as a $z \sim 7$ source for which we already have a wealth of resolved information despite the limited amount of telescope time invested. We explore the current uncertainties and make predictions of what *JWST* will be able to see for CR7 under different scenarios/assumptions, allowing us to identify what are the key lines that will differentiate between different physical interpretations in each individual clump.

Table 2. A summary of the high ionisation rest-frame UV lines investigated for CR7 and/or their upper limits constrained in this work; see also Veilleux (2002). We list and use them in vacuum. We list either clear detections ($> 3\,\sigma$), tentative detections ($\sim 2-3\,\sigma$, accompanied by the $1\,\sigma$ error and the central value $+\,2\,\sigma$ upper limit) or we list the $< 2\,\sigma$ non-detections constraints for the "full system" and also for each of the clumps A, B, C. We use these to constrain/contrast with our CLOUDY modelling and infer potential physical conditions with CR7 and the individual clumps. *Lyα flux from the X-SHOOTER slit (observed) implies $5.9 \pm 0.5 \times 10^{-17}$ erg s^{-1} cm^{-2}, with a slit and seeing of $\approx 0.9''$, which suggests the slit should recover $\sim 68\%$ of a point-like source – we apply this slit correction to all X-SHOOTER flux limits. Lyα is clearly extended, and thus the actual full slit losses would have to be larger, but here we apply the $\sim 1/0.68$ slit correction for slit fluxes. We also assume that the slit (point-like corrected) is able to recover roughly the full Lyα flux associated with clump A. Based on the 2D Lyα distribution from NB photometry, we assume that B has a flux $\sim 40\%$ of A and C $\sim 30\%$ of A, but note that these Lyα fluxes have not been measured directly with spectroscopy, and are thus very uncertain.

Emission line $\lambda_{\rm vacuum}$ (Å)	Ionisation Energy (eV)	Line Flux Full 10^{-17} erg s^{-1} cm^{-2}	Clump A	Clump B	Clump C	Instruments Used for flux
Lyα 1215.67	13.6	17 ± 1 [8.7 ± 0.7 slit]	$9 \pm 1^*$	$3.3 \pm 1.0^*$	$2.6 \pm 1.0^*$	XSH
N V 1238.8,1242.78	77.4	< 0.9 [1.3 ± 0.5 OB3]	–	–	[1.3 ± 0.5?]	XSH
O IV] 1401,1407	54.9	< 2.2	–	–	–	XSH
N IV] 1483.4,1486.6	47.4	< 3.2	1.5 ± 0.7 (< 2.7)	< 0.7	< 1.5	XSH+WFC3
C IV 1548.2,1550.77	47.9	< 1.4	< 1.5	< 1.5	< 0.7	XSH+WFC3
He II 1640.47	54.4	< 4.7 [2.6 ± 1.0 OB3]	< 0.5	< 0.6	1.0 ± 0.4 (< 1.7)	XSH+WFC3
O III] 1661,1666	35.1	< 1.5	< 1.1	< 2.2	< 0.8	XSH+WFC3
N III] 1749.7,1752.2	29.6	< 1.1	< 1.3	< 0.4	< 0.9	XSH+WFC3
C III] 1907,1910	24.4	< 2.7	< 0.7	< 0.4	< 1.0	XSH+WFC3
Mg II 2796,2803	7.6	< 1.3	–	–	–	XSH

Table 3. Parameters and ranges used for our CLOUDY (Ferland et al. 1998, 2013) modelling (Alegre et al. in prep.). We vary density, metallicity and the ionisation parameter for both the star-like ionisation (here modelled with a black body of varying temperature from 20 to 150K)[1] and for an AGN-like ionisation (here modelled with a power-law slope[2]). We also use the latest BPASS[3] (Eldridge & Stanway 2009; Stanway et al. 2016) models.

Parameter	**Range used for all models**
Density ($n_{\rm H}$ cm^{-3})	100
Metallicity ($Z_\odot$)	0.001, 0.01, 0.1, 1
Ionisation param. ($\log U$)	-4, -3, -2, -1
Type of model	**Range used**
Black body[1] (Temp.)	20kK to 150kK (steps of 10kK)
Power-law[2] (slope)	-1.2, -1.4, -1.6, -1.8, -2.0
BPASS[3] (log Age, yr)	5.9-8.0 (steps of 0.4 dex)

4.1 CLOUDY modelling

In order to explore a relatively wide range of physical conditions that may be happening in CR7, we use the CLOUDY (v 13.03) photo-ionisation code (Ferland et al. 1998, 2013). Full details are given in Alegre et al. (in prep.). Table 3 summarises the key physical conditions. Briefly, we use three kinds of models (for a similar, more extensive analysis, see also, e.g. Nakajima et al. 2017): i) power-laws to mimic the spectra of AGN, ii) stellar spectra from BPASS (Eldridge & Stanway 2009; Eldridge et al. 2017; Stanway et al. 2016) and iii) black body models to further interpret and make simple predictions. We note that as a first step, and for simplicity, we only ionise the gas using photons. Shock ionisation may in principle also play a role (e.g. Allen et al. 2008; Jaskot & Ravindranath 2016), which could be explored once observations provide detections in a range of lines, and particularly to explore spatially resolved emission-line ratio maps (see e.g. Miley & De Breuck 2008; Morais et al. 2017; Comerford et al. 2017).

By using our large grid of models, we produce synthetic spectra which we use to compare with our observations and test which physical conditions/models we can reliably exclude and which ones are still consistent with CR7. In order to constrain the potential physical conditions in CR7, we use the full CLOUDY grid for each of the models and use all line ratios that involve at least one detected line. This allows us to either exclude specific ranges of line ratios (and thus exclude specific physical conditions), if one of the lines is only an upper limit, or to use the $1\,\sigma$ values of each line (in the case of detection) to select all potential models that satisfy a given line ratio, resulting in a range of possible physical conditions. We then look at the physical conditions that are consistent with the current line ratio constraints and exclude those that are clearly inconsistent. We stress that our aim is not to claim "true" physical conditions, but rather to broadly identify what physical conditions may be present in CR7.

4.2 The physical conditions in CR7 with current constraints: the full system

We use our simple CLOUDY grid predictions to interpret what the current measurements and constraints of several lines in CR7 imply. We start by looking at the full CR7 system as a whole using flux measurements from X-SHOOTER and three different cases: when we assume that only He II is detected, when assuming that only N V is detected, and when assuming that both He II and N V are detected. We note that if one assumes that no line is detected apart from Lyα and only upper limits are used, models are, not surprisingly, mostly unconstrained. However, we note that the extremely luminous Lyα detection, together with good constraints of the total SFR for CR7 (including dust corrected UV luminosity with direct measurements of the dust IR luminosity), implies close to 100% Lyα escape fraction for the system

Table 4. Rest-frame EW limits for UV lines (see Table 2) inferred from our WFC3 grism observations of each of the three UV clumps of CR7. We use the flux limits provided in Table 2 and UV luminosities of −21.7, −20.0 and −20.1 for clumps A, B and C, respectively. We list either tentative detections ($\sim 2-3\,\sigma$, accompanied by the $1\,\sigma$ error and the central value + $2\,\sigma$ upper limit) or we list the $< 2\,\sigma$ non-detections constraints.

Emission Line	Clump A (Å)	Clump B (Å)	Clump C (Å)
NIV]	30 ± 25 (< 55)	< 70	< 140
CIV	< 30	< 150	< 60
HeII	< 10	< 60	90 ± 60 (< 150)
OIII]	< 25	< 220	< 70
NIII]	< 30	< 40	< 80
CIII]	< 30	< 40	< 90

Table 5. Best-fit physical properties from current constraints of CR7 and its UV components. SFRs are taken from Matthee et al. (2017a), while for β we combine constraints from photometry and our grism spectra. Current constraints are consistent with ionisation parameters ($\log U$) of ~ -3.0 for clump A and ~ -2.5 for clump C, while for B it is completely unconstrained. Given the constraints/upper limits of rest-frame UV lines, we estimate potential gas-phase metallicities in the range $\sim 0.05-0.2\,Z_\odot$; *JWST* observations will be crucial to measure these directly.

CR7 Component	SFR ($M_\odot\,yr^{-1}$)	β	Likely dom. nature
Full	45 ± 2	-2.2 ± 0.4	Star-burst
A	28^{+2}_{-1}	-2.4 ± 0.4	Star-burst
B	5^{+2}_{-1}	-1.6 ± 0.8	Star-burst
C	7^{+1}_{-1}	-2.4 ± 0.8	Star-burst/AGN

as a whole, and allows a further constraint on the allowed conditions so they do not violate the SFR constraints. We show our results in Table 5.

If we assume that HeII is real in the system as a whole (implying a rest-frame EW of 35 ± 20 Å; see Tables 2 and 4), we find that BPASS models can reproduce the observations relatively well if the metallicity of the gas is $\approx 0.05-0.1\,Z_\odot$ (see also Bowler et al. 2017b). CR7 as a whole may therefore be explained as a $\sim 10-50$ Myr burst with a metallicity of $\approx 0.1\,Z_\odot$. For this scenario our power-law and black body models also easily reproduce the observations, implying gas-phase metallicities of $\approx 10-20\%$ solar and ionisation parameters of $\log U \approx -2.8$. We note, nonetheless, that a large range of physical conditions are still possible, even in the limited parameter space that we have explored.

Assuming that NV is real but using HeII as an upper limit has very strong effects in the interpretation of the system as a whole (although see discussion as NV, if real, is not likely to come from e.g. clump A, as it is significantly blue-shifted). BPASS models fail to match the line ratios that involve NV, and thus not surprisingly the power-law models perform much better. In this case we expect a very high ionisation parameter potentially in excess of $\log U \approx -1$. Assuming that both HeII and NV are real in the system would lead to similar conclusions as taking HeII as an upper limit and would still imply an AGN nature, a very high ionisation parameter, and a roughly solar gas metallicity (but see also Matsuoka et al. 2009, 2017) for the power-law models.

4.3 CR7 resolved: the nature of each individual UV clump

Next, we focus on the resolved results and study clumps A, B and C individually. For clump B the current flux and EW upper limits (Tables 2 and 4) do not allow to truly constrain the physical conditions that we explore, but we note that ALMA results hint for a metallicity of $\approx 0.1-0.2\,Z_\odot$ (based on the [CII]/UV ratio; Matthee et al. 2017a), while our non-detection of any high ionisation lines in clump B does not provide any evidence for an unusually high ionisation parameter or for strong AGN activity, given the limits on the EW of CIII] (see e.g. Nakajima et al. 2017), although some AGN activity is still possible. We further constrain the physical conditions using the UV+FIR SFR measured per clump (Matthee et al. 2017a), not allowing models to significantly over or underestimate by factors of more than two the SFR per clump.

For clump A, the tentative detection of NIV] (with a potential EW of 30 ± 25 Å) and the strong non-detections of other lines, including HeII (EW< 10 Å) allows to place some constraints on the nature of the source. With current observations, and even if NIV] is taken as real in clump A, there is no strong evidence for the presence of an AGN, as stellar models (particularly at lower metallicities and/or with binaries) can easily reproduce the emission line ratios with $\log U \approx -3$, a gas-phase metallicity of $\sim 5-20\%$ solar and a relatively young burst of $\sim 10-30$ Myrs. We therefore conclude that even in the presence of NIV] (at the level measured, and given the large errors and the strong continuum from A), the non-detection of HeII and any other high ionisation line in clump A suggest the source is powered by a $\sim 10-30$ Myr star-burst of $\sim 10-20\%$ solar metallicity.

For clump C, the potential detection of HeII (with a potential rest-frame EW of 90 ± 60 Å) brings in some evidence of its potential AGN nature, while the non-detections of the other lines are also consistent with a potential AGN nature. By using all constraints, models suggest that C can be powered by an ionisation source with roughly $\log U \approx -2.5$, with a lower Lyα escape fraction than clumps A and B, and surrounded by a relatively low metallicity gas, but the constraints are currently very weak. If NV is found in clump C, or if we associate the potential blue-shifted NV line as coming from or around clump C, then the source would be more definitively identified as a high ionisation source powered by an AGN (e.g. Matsuoka et al. 2009). Deeper NV observations centred on clump C are necessary for this.

We conclude that with the current uncertainties (see Table 5), all three clumps are consistent with being relatively young star-bursts with similar gas-phase metallicities of $\sim 0.05-0.2\,Z_\odot$. There is currently no strong evidence for the presence of an AGN in either clumps A or B, and there is only tentative evidence for clump C to have a higher ionisation parameter and to potentially host an AGN. However, the physical proximity of clumps A and B to C could potentially affect their nebular spectra and even make those variable, particularly if C is a high ionisation source and ionising photons reach out into the gas surrounding A or B.

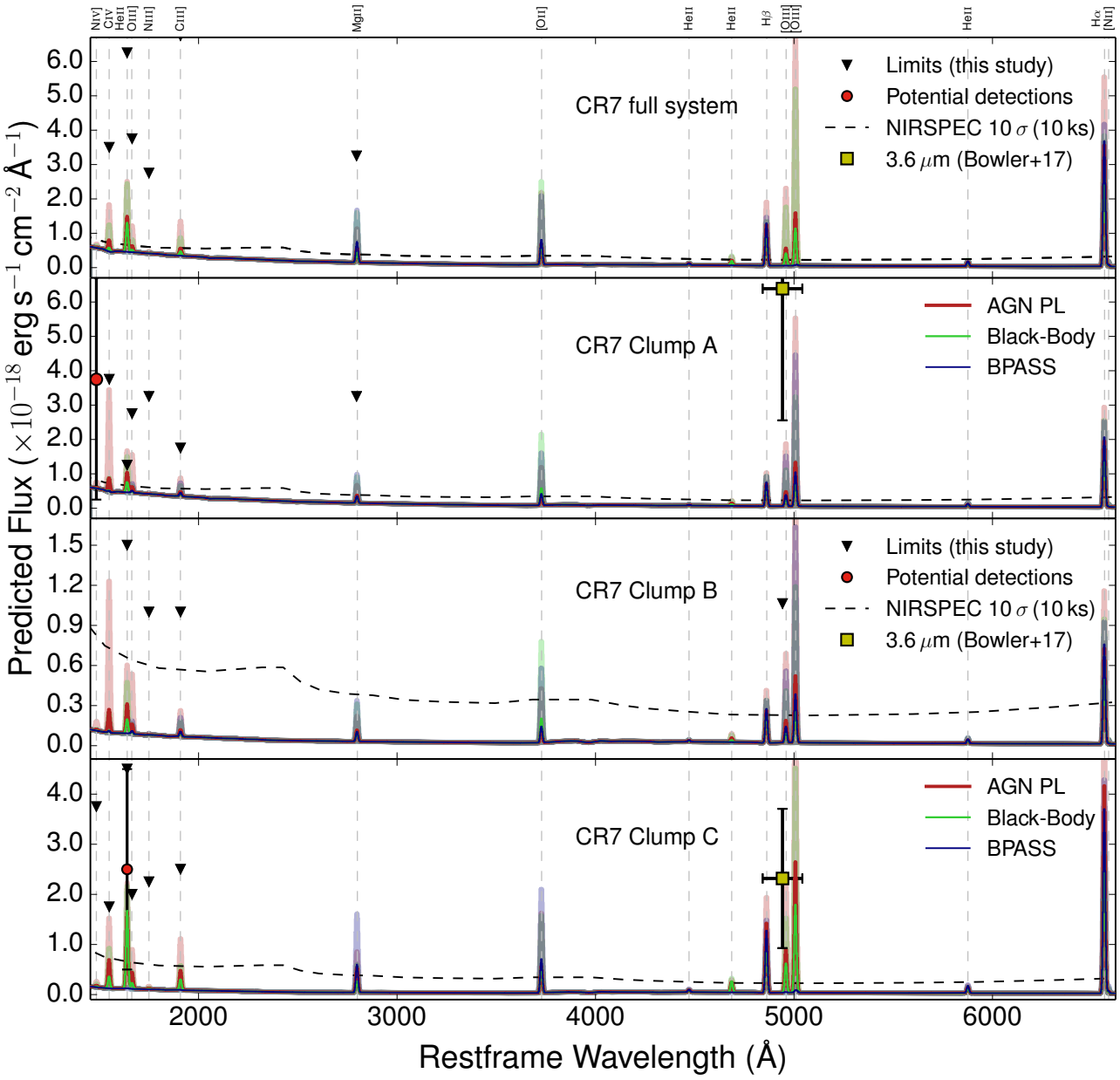


Figure 10. Predictions for *JWST*/NIRSpec observations for each of the 3 clumps in the rest-frame UV and in the rest-frame optical. We show the predictions from CLOUDY with current constraints and also showing the current best continuum fits from Bowler et al. (2017b). In addition to the best flux limits for various lines, we also show the current estimates on potential ~ 5000 Å emission line flux from Spitzer derived by Bowler et al. (2017b) (which here we assume is split in 3 lines equally to compare with predictions), but we do not use those to constrain the models. Even though they agree well with out predictions, there may be hints that a larger fraction of the Spitzer flux may come from clump C and a lower fraction from clump A. For reference, we show the $10\,\sigma$ detection limit for NIRSpec with an integration of 10 ks. We find that such integration will easily be able to distinguish between the various physical conditions that are still possible for each of the clumps, and particularly constrain the nature, metallicity and dust extinction of clump A very accurately. These observations will also easily identify any AGN presence in any of the clumps, particularly for clumps B and C (with BPT or by identifying significant HeII and CIV emission, for example). Hα should be the strongest line in any of the spectra, but it is possible that [OIII]5007 is at least as strong, if not stronger. We also find that while clumps A and B are well described with a Lyα escape fraction close to 100%, for clump C it is likely that the escape fraction is significantly lower ($\sim 10-30\,\%$).

4.4 Predictions for JWST under different scenarios

Given the constraints presented in Section 4.3 for each clump, we now explore what they imply in terms of the various emission lines that *JWST* will be able to trace: not only because it will be able to access the rest-frame optical, but also because it will be able to probe deeper in the rest-frame UV. CR7 has been announced as a GTO target for *JWST*/NIRSpec, and should be observed with the IFU. Of particular importance are observations in the rest-frame optical in the range e.g. $2.87-5.27\,\mu$m, which

will be able to trace many of the main rest-frame optical lines ($3776 - 6934$ Å) with $R \sim 1000$, which results in emission lines with $\sigma \sim 40$ Å or $\approx 300\,\mathrm{km\,s^{-1}}$ (FWHM of $\approx 700\,\mathrm{km\,s^{-1}}$). Other disperser/filter combinations can be used and will allow the complete probing of emission lines from Lyα to beyond Hα, resolving the properties of each of the 3 clumps and any gas in between them. Such observations will provide the community with the most detailed view ever obtained of a galaxy into the epoch of re-ionisation at $z \sim 7$, including the inter-clump medium of CR7.

We use the best continuum constraints and those presented in Bowler et al. (2017b) (continuum fits to each individual clump) for each of the clumps to which we add emission lines from our CLOUDY modelling and we compare those with the current best limits from this paper and also constraints from Bowler et al. (2017b) based on Spitzer photometry. We show the results in Figure 10 and also in Table 6. We find that current constraints still allow for a relatively large range of emission line fluxes in the rest-frame optical. Most importantly, our predictions clearly show how a "standard" integration of 10 ks with NIRSpec will be able to significantly detect ($> 10\,\sigma$) at least Hα, [OIII], Hβ, potentially [OII] and even MgII for clump A, and thus fully unveiling its Lyα escape fraction, dust extinction, metallicity, ionisation parameter and revealing any weak AGN activity within it. *JWST* IFU observations of CR7 will also allow to unveil the presence of an AGN in either B or C, along with determining (albeit with slightly larger errors than A) their metallicities, dust extinction and at least place a lower limit in the ionisation parameter. Our results are thus a good guideline for what may be expected from *JWST* observations of CR7.

5 DISCUSSION

CR7 has previously been discussed as being powered by very low metallicity stars (PopIII-like; Sobral et al. 2015; Visbal et al. 2016), as a candidate for being a DCBH (e.g. Sobral et al. 2015; Pallottini et al. 2015; Hartwig et al. 2016; Agarwal et al. 2016, 2017), or as hosting a significant population of young, binary stars and/or WR stars at extremely low metallicities (e.g. Bowler et al. 2017b). The observed Lyα and HeII EWs based on photometry in Sobral et al. (2015) could only be explained by an extreme hard ionising spectrum, implying a high effective temperature and an extremely low metallicity of $\approx 0.05 - 0.5\,\%$ solar (Hartwig et al. 2016; Bowler et al. 2017b). Different components of CR7 have now been spectroscopically confirmed to be part of the same system (Matthee et al. 2017a), with velocity offsets of only a few hundred $\mathrm{km\,s^{-1}}$ at most, and with some evidence of dynamics/potential merging activity. New observations of CR7 clearly reveal the unique potential of bright enough targets at high redshift, allowing the first spatially resolved studies of both rest-frame UV lines and [CII] detections with ALMA (Matthee et al. 2017a).

Overall, and specifically for clump A, our results show that the HeII/Lyα ratio is significantly lower than measured using UltraVISTA flux estimate of HeII (Sobral et al. 2015), with this ratio being below $\sim 0.05 - 0.06$ instead of close to ~ 0.2. This rules out the most extreme DCBH scenarios for clump A. Together with the [CII] detection in A (Matthee et al. 2017a), our results imply a metallicity of roughly 0.1-0.2 $\mathrm{Z_\odot}$ for clump A (to be confirmed/verified with *JWST*), thus becoming globally inconsistent with a "PopIII-like" scenario metallicity ($\sim 0.005\,\mathrm{Z_\odot}$; Bowler et al. 2017b). Our latest results indicate that A is a more 'normal' starburst, consistent with feedback processes already fully in place, as indicated from the Lyα line profile modelling (Dijkstra et al. 2016). It is interesting that while ALMA provides a detection of Carbon (Matthee et al. 2017a) in CR7's clump A (also in/around clumps B and C), and even though we estimate a metallicity of roughly 0.1-0.2 $\mathrm{Z_\odot}$ (similar to sources studied by e.g. Stark et al. 2015), we do not detect any high ionisation Carbon line (e.g. CIV or CIII]), down to rest-frame EW upper limits of $\approx 16, 25$ Å in CIII] and CIV, respectively. This is consistent with the hypothesis explored in Matthee et al. (2017c) that current CIV and CIII] detections in galaxies at the epoch of re-ionisation are only possible for even brighter sources with much higher observed SFRs (UV brighter or with significant lensing amplifications) and/or AGN.

Our results tentatively highlight CR7's clump C as the most puzzling and uncertain at the moment. This component seems to show the largest blueshift, and might be associated with a potential blue-shifted ($z = 6.583 \pm 0.001$) NV detection. Furthermore, HeII is also tentatively detected on or near clump C. The fact that we find no significant UV continuum detection for clump C with our *HST* grism observations, but detect clump B in the rest-frame UV (from photometry taken on March 2012 clump C was fainter than B, see e.g. Bowler et al. 2017b) suggests that clump C may be variable, and has become fainter by $\sim 0.2 - 0.4$ mag when compared to previous *HST* observations. This could also indicate that any potential emission lines from C have also become weaker. While there are indications that C may host an AGN/high ionisation UV source, this would be somewhat puzzling in other regards as it would imply a likely low black hole mass given its sub-L* luminosity in both observed Lyα and in the UV (in our grism observations it is the faintest component in CR7). While some obscuration could in principle be invoked to explain the low luminosity in Lyα and the UV for clump C, ALMA observations (Matthee et al. 2017a) do not detect any dust, although one should mention that they are not so sensitive to significantly hot dust that may be present in C. As for Lyα being apparently very weak near clump C, it may be a consequence of its velocity and the significant blueshift when compared to the observed Lyα emission, which may lead to Lyα photons only escaping after significant scattering which may lead to an important apparent spatial offset.

In principle, future X-ray observations may also help to determine the nature of these high redshift sources, but these may have to achieve significantly high resolution (if they are to locate AGN within multi-component galaxies) and be relatively deep to detect the presence of an AGN in e.g. clump C. Given its luminosity in the UV and also its potential NV and HeII luminosities, one would expect X-ray luminosities of $\approx 10^{42}\,\mathrm{erg\,s^{-1}}$, about ~ 4 times lower than predicted by Pallottini et al. (2015) due to the much lower HeII luminosity in clump C than originally estimated for CR7 as a whole using UltraVISTA photometry (Sobral et al. 2015). Therefore, identifying AGN will likely be much more efficient with *JWST*, particularly with the IFU on NIRSpec.

Our results also point towards potential consequences when interpreting emission lines from clump C and from

Table 6. Best-fit predictions for rest-frame optical emission lines, currently inaccessible. All fluxes are in units of 10^{-18} erg s^{-1} cm^{-2} and should be affected by a Lyα escape fraction term, i.e., if the escape fraction is not 1.0 then a correction of $1/f_{esc,Ly\alpha}$ should be applied. For clumps A and B $f_{esc,Ly\alpha}$ is expected to be close to ~ 1, while for C there are indications that it may be closer to ~ 0.15, so the emission line fluxes may be ~ 7 times higher than provided here. Constraining these lines with *JWST* will allow to not only improve our understanding of physical conditions in $z \sim 7$ galaxies like CR7 in a resolved way, but also start to understand the potential link between the different ionising sources, gas, metallicities and dust in the hosts of likely early ionised bubbles within the epoch of re-ionisation.

CR7	[OII]3727	HeII4471	HeII4686	Hβ	[OIII]4959	[OIII]5007	HeII5016	HeII5876	Hα	[NII]6584
A	3.0 ± 2.0	0.11 ± 0.04	$0.001 - 0.4$	3.0 ± 0.5	$0.7 - 6.0$	$2 - 17$	0.07 ± 0.02	0.3 ± 0.1	8.9 ± 1.1	0.15 ± 0.12
B	1.0 ± 0.5	0.03 ± 0.01	$0.0004 - 0.2$	0.7 ± 0.2	0.7 ± 0.5	2.0 ± 1.7	0.02 ± 0.01	0.08 ± 0.02	2.0 ± 0.4	0.04 ± 0.03
C	1.0 ± 0.3	0.03 ± 0.01	$0.001 - 0.2$	0.7 ± 0.1	$0.01 - 0.8$	$0.03 - 2.3$	0.02 ± 0.01	0.08 ± 0.01	2.3 ± 0.3	0.07 ± 0.02

other clumps/the full system. Given the geometry of the system and the small velocity offsets between components (see Matthee et al. 2017a), the potential AGN nature of clump C and its variability, it is possible that each clump is differentially illuminated by a time-dependent AGN+SF composite SED. Observations with *JWST* obtained over $\sim 1-2$ years would be crucial to test how important any time-variability and the illumination from different clumps may be. This would be important to e.g. understand whether illumination from another clump (e.g. C) could give rise/be responsible for potential high ionisation lines seen in the gas of another (e.g. the potential NIV] detection in clump A). Until then, detailed 3D simulations could be performed with full radiation transfer in order to further investigate similar systems and allow to make specific predictions, not only for CR7, but for other similar sources within the epoch of re-ionisation.

Overall, it seems that each individual clump is consistent with roughly the same metallicity of roughly 10 to 20% solar, although there is marginal evidence for clump B to be slightly more metal rich (closer to 20% solar) and for clumps A and C to be slightly more metal poor (closer to 5-10% solar). *JWST* will be able to measure accurately the metallicity of each clump and clearly show if there are spatial variations within CR7. If such metallicity differences are found, it could also highlight potential recent gas accretion closer to clumps A and C and further away from B.

6 CONCLUSIONS

We presented new *HST*/WFC3 grism observations and combined those with a re-analysis of X-SHOOTER and SINFONI data obtained on the VLT to unveil the continuum, variability and rest-frame UV lines of the 3 UV components of the most luminous Lyα emitter at $z = 6.6$, COSMOS Redshift 7 (CR7; Sobral et al. 2015). We find that:

- Our re-reduced, flux calibrated X-SHOOTER and SINFONI spectra of CR7 reveals a low significance detection of HeII with a flux of $F_{HeII} = (1.8 \pm 0.7) \times 10^{-17}$ erg s^{-1} cm^{-2}. We identify the HeII signal ($\sim 2.6\,\sigma$, suggesting a rest-frame EW of 35 ± 20 Å) as coming only from observations obtained along the major axis of Lyα emission. The observations with the tentative HeII signal also show a potential NV detection for $z = 6.583 \pm 0.001$, hinting for a blue-shifted component potentially ionised by an AGN which ALMA data locate closer to clump C.
- We find a change of +0.2-0.5 mag in UltraVISTA *J* band data for CR7 as a whole from DR2 to DR3, which virtually eliminates the strong *J*-band excess interpreted as being caused by HeII. While this is a large change, it is not statistically significant due to large variations in UltraVISTA data from DR2 to DR3 for other sources.
- Our WFC3 grism spectra provide a significant detection of the UV continuum of CR7's clump A, yielding an excellent fit to a power law with $\beta = -2.4 \pm 0.4$ and $M_{UV} = -21.7 \pm 0.3$. This is fully consistent with the broad band photometry, and with no variability within ~ 0.4 mag. We detect weak continuum in clump B but fail to detect continuum in clump C, which from photometry is brighter than B. This hints for potential variability in clump C.
- In our *HST* Grism data we do not detect any rest-frame UV line in clump A above $3\,\sigma$ and find $F_{HeII} < 0.5 \times 10^{-17}$ erg s^{-1} cm^{-2} at a 2σ level (HeII EW$<$ 10 Å). We find a tentative ($\sim 2\,\sigma$) NIV] detection in clump A, but this requires further observations. We do not find any evidence of even weak UV rest-frame emission lines in clump B, with rest-frame EW limits varying from <40 to <200 Å.
- Our results show that the HeII/Lyα ratio is significantly lower than measured using UltraVISTA flux estimate of HeII (Sobral et al. 2015), with this ratio being below $\sim 0.05-0.06$ instead of close to ~ 0.2. This rules out the most extreme DCBH scenarios for clump A.
- We tentatively identify C as a potential high ionisation source with $F_{HeII} = (1.0 \pm 0.4) \times 10^{-17}$ erg s^{-1} cm^{-2}, which would imply a rest-frame EW of 90 ± 60 Å. Together with the evidence of variability, our observations suggest that clump C may be powered by an AGN.
- We perform CLOUDY modelling and obtain limits on the metallicity and constrain the ionising nature of CR7, and also make predictions for *JWST*/NIRSpec. We conclude that CR7 is likely actively forming stars without any clear AGN activity in clumps A and B, with a metallicity of $\sim 0.1 - 0.2\,Z_\odot$ (to be confirmed/verified with *JWST*) and with component A experiencing the most massive starburst. Together with the [CII] detection in clumps A and B (Matthee et al. 2017a), our results are globally inconsistent with a "PopIII-like" scenario metallicity ($\sim 0.005\,Z_\odot$; Bowler et al. 2017b) for clumps A and B.
- Component C may host a high ionisation source/AGN, be potentially more metal poor, and may well be variable. Our results thus highlight the need for spatially resolved information (and time variability constraints) to study the complex formation and assembly of galaxies within the epoch of re-ionisation.

Overall, our results reveal that CR7 is a complex sys-

tem which may be giving us an early glimpse of the complicated processes taking place in the early Universe. The high resolution observations presented here (capable of investigating the system in its 3 UV clumps), those obtained by ALMA (e.g. Jones et al. 2017b; Matthee et al. 2017a) and recent simulations for galaxies at $z \sim 7$ (e.g. Gallerani et al. 2016) point towards early galaxies being chaotic collections of metal-poor merging clumps which will also likely bring along black holes. Such complex systems imply that the approach of simply placing a very narrow slit in a given UV light peak may only reveal part of the full picture, particularly if there is significant ionising flux from nearby sources. Indeed, it seems that the systems studied so far at $z \sim 7$ require spatially resolved observations, ideally obtained by IFU spectrographs, in order to identify the nature of different components. Furthermore, the potential hints of variability in one of the clumps in CR7 (C) and its potential AGN nature, also highlights a further important complication: the role of time variability in any conclusions that may be drawn. The current results also reveal the importance of simulations to take into account such complex systems by performing a full 3D radiation transfer for systems like CR7 and comparing with observations, particularly to constrain the role of multiple ionising sources. Until *JWST* is fully operational, further spatially resolved observations of other bright enough systems (e.g. Himiko, MASOSA, VR7; Ouchi et al. 2013; Sobral et al. 2015; Matthee et al. 2017c) with MUSE, ALMA and *HST* will assure an even more efficient laboratory to advance our knowledge of the early assembly of galaxies within the epoch of re-ionisations which can then be further applied to fainter and more numerous sources.

ACKNOWLEDGMENTS

DS acknowledges financial support from the Netherlands Organisation for Scientific research (NWO) through a Veni fellowship. JM acknowledges the support of a Huygens PhD fellowship from Leiden University. AF acknowledges support from the ERC Advanced Grant INTERSTELLAR H2020/740120. BD acknowledges financial support from NASA through the Astrophysics Data Analysis Program (ADAP), grant number NNX12AE20G.

Based on observations obtained with *HST*/WFC3 program 14495. Based on observations of the National Japanese Observatory with the Suprime-Cam on the Subaru telescope (S14A-086) on the big island of Hawaii. This work is based in part on data products produced at Terapix available at the Canadian Astronomy Data Centre as part of the Canada-France-Hawaii Telescope Legacy Survey, a collaborative project of NRC and CNRS. Based on data products from observations made with ESO Telescopes at the La Silla Paranal Observatory under ESO programme IDs 294.A-5018, 294.A-5039, 092.A-0786, 093.A-0561, 097.A-0943, 098.A-0819 and 179.A-2005, and on data products produced by TERAPIX and the Cambridge Astronomy Survey Unit on behalf of the UltraVISTA consortium. The authors acknowledge the award of service time (SW2014b20) on the William Herschel Telescope (WHT). WHT and its service programme are operated on the island of La Palma by the Isaac Newton Group in the Spanish Observatorio del Roque de los Muchachos of the Instituto de Astrofisica de Canarias.

We have benefited immensely from the public available programming language Python, including NumPy & SciPy (Van Der Walt et al. 2011; Jones et al. 2001), Matplotlib (Hunter 2007), Astropy (Astropy Collaboration et al. 2013) and the Topcat analysis program (Taylor 2013). This research has made use of the VizieR catalogue access tool, CDS, Strasbourg, France.

Data used for this paper are publicly available, and we make all reduced data available with the refereed paper.

REFERENCES

Agarwal B., Johnson J. L., Zackrisson E., Labbe I., van den Bosch F. C., Natarajan P., Khochfar S., 2016, MNRAS, 460, 4003
Agarwal B., Johnson J. L., Khochfar S., Pellegrini E., Rydberg C.-E., Klessen R. S., Oesch P., 2017, MNRAS, 469, 231
Allen M. G., Groves B. A., Dopita M. A., Sutherland R. S., Kewley L. J., 2008, ApJS, 178, 20
Astropy Collaboration et al., 2013, A&A, 558, A33
Bouwens R. J., et al., 2014, ApJ, 793, 115
Bouwens R. J., Smit R., Labbé I., Franx M., Caruana J., Oesch P., Stefanon M., Rasappu N., 2016, ApJ, 831, 176
Bowler R. A. A., et al., 2012, MNRAS, 426, 2772
Bowler R. A. A., et al., 2014, MNRAS, 440, 2810
Bowler R. A. A., et al., 2017a, MNRAS, 466, 3612
Bowler R. A. A., McLure R. J., Dunlop J. S., McLeod D. J., Stanway E. R., Eldridge J. J., Jarvis M. J., 2017b, MNRAS, 469, 448
Brammer G. B., et al., 2012, ApJS, 200, 13
Brammer G., Pirzkal N., McCullough P., MacKenty J., 2014, Technical report, Time-varying Excess Earth-glow Backgrounds in the WFC3/IR Channel
Capak P. L., et al., 2015, Nature, 522, 455
Carniani S., Maiolino R., Pallottini A., et al., 2017, A&A, 605, A42
Comerford J. M., Barrows R. S., Müller-Sánchez F., Nevin R., Greene J. E., Pooley D., Stern D., Harrison F. A., 2017, preprint, (arXiv:1710.00825)
Dijkstra M., Gronke M., Sobral D., 2016, ApJ, 823, 74
Dunlop J. S., McLure R. J., Robertson B. E., Ellis R. S., Stark D. P., Cirasuolo M., de Ravel L., 2012, MNRAS, 420, 901
Eldridge J. J., Stanway E. R., 2009, MNRAS, 400, 1019
Eldridge J. J., Stanway E. R., 2012, MNRAS, 419, 479
Eldridge J. J., et al., 2017, preprint, (arXiv:1710.02154)
Erb D. K., Pettini M., Shapley A. E., Steidel C. C., Law D. R., Reddy N. A., 2010, ApJ, 719, 1168
Faisst A. L., Capak P., et al., 2016, ApJ, 821, 122
Ferland G. J., Korista K. T., Verner D. A., Ferguson J. W., Kingdon J. B., Verner E. M., 1998, PASP, 110, 761
Ferland G. J., et al., 2013, RMAA, 49, 137
Gallerani S., Pallottini A., Feruglio C., Ferrara A., Maiolino R., Vallini L., Riechers D. A., 2016, preprint, (arXiv:1604.05714)
Gräfener G., Vink J. S., 2015, A&A, 578, L2
Gronke M., 2017, preprint, (arXiv:1709.07008)
Hartwig T., et al., 2016, MNRAS, 462, 2184
Hayes M., Schaerer D., Östlin G., Mas-Hesse J. M., Atek H., Kunth D., 2011, ApJ, 730, 8
Hu E. M., Cowie L. L., Songaila A., Barger A. J., Rosenwasser B., Wold I. G. B., 2016, ApJL, 825, L7
Hu W., et al., 2017, preprint, (arXiv:1706.03586)
Hunter J. D., 2007, Computing In Science & Engineering, 9, 90
Jaskot A. E., Ravindranath S., 2016, ApJ, 833, 136
Jones E., Oliphant T., Peterson P., et al., 2001, SciPy: Open source scientific tools for Python, http://www.scipy.org/
Jones G. C., et al., 2017a, preprint, (arXiv:1709.04954)

Jones G. C., Willott C. J., Carilli C. L., Ferrara A., Wang R., Wagg J., 2017b, ApJ, 845, 175
Karman W., Caputi K. I., Caminha G. B., Gronke M., et al., 2017, A&A, 599, A28
Khostovan A. A., Sobral D., Mobasher B., Smail I., Darvish B., Nayyeri H., Hemmati S., Stott J. P., 2016, MNRAS, 463, 2363
Kuntschner H., Bushouse H., Kümmel M., Walsh J. R., MacKenty J., 2010, in Space Telescopes and Instrumentation 2010: Optical, Infrared, and Millimeter Wave. p. 77313A, doi:10.1117/12.856421
Laporte N., Nakajima K., Ellis R. S., Zitrin A., Stark D. P., Mainali R., Roberts-Borsani G., 2017, preprint, (arXiv:1708.05173)
Maiolino R., et al., 2015, MNRAS, 452, 54
Mármol-Queraltó E., McLure R. J., Cullen F., Dunlop J. S., Fontana A., McLeod D. J., 2016, MNRAS, 460, 3587
Matsuoka K., Nagao T., Maiolino R., Marconi A., Taniguchi Y., 2009, A&A, 503, 721
Matsuoka K., Nagao T., Maiolino R., Marconi A., Park D., Taniguchi Y., 2017, preprint, (arXiv:1709.07000)
Matthee J., Sobral D., Santos S., Röttgering H., Darvish B., Mobasher B., 2015, MNRAS, 451, 400
Matthee J., et al., 2017a, preprint, (arXiv:1709.06569)
Matthee J., Sobral D., Best P., Khostovan A. A., Oteo I., Bouwens R., Röttgering H., 2017b, MNRAS, 465, 3637
Matthee J., Sobral D., Darvish B., Santos S., Mobasher B., Paulino-Afonso A., Röttgering H., Alegre L., 2017c, MNRAS, 472, 772
McCracken H. J., et al., 2012, AAP, 544, A156
McGreer I. D., et al., 2017, preprint, (arXiv:1706.09428)
Miley G., De Breuck C., 2008, A&ARv, 15, 67
Modigliani A., et al., 2010, in Observatory Operations: Strategies, Processes, and Systems III. p. 773728, doi:10.1117/12.857211
Momcheva I. G., et al., 2016, ApJS, 225, 27
Morais S. G., et al., 2017, MNRAS, 465, 2698
Nakajima K., Ouchi M., 2014, MNRAS, 442, 900
Nakajima K., Schaerer D., Le Fevre O., Amorin R., et al., 2017, preprint, (arXiv:1709.03990)
Ota K., et al., 2014, ApJ, 792, 34
Ouchi M., et al., 2013, ApJ, 778, 102
Pacucci F., Pallottini A., Ferrara A., Gallerani S., 2017, MNRAS, 468, L77
Pallottini A., et al., 2015, MNRAS, 453, 2465
Pentericci L., et al., 2014, ApJ, 793, 113
Salpeter E. E., 1955, ApJ, 121, 161
Santos S., Sobral D., Matthee J., 2016, MNRAS, 463, 1678
Schaerer D., Boone F., Zamojski M., Staguhn J., Dessauges-Zavadsky M., Finkelstein S., Combes F., 2015, AAP, 574, A19
Schenker M. A., Stark D. P., Ellis R. S., Robertson B. E., Dunlop J. S., McLure R. J., Kneib J.-P., Richard J., 2012, ApJ, 744, 179
Schenker M. A., Ellis R. S., Konidaris N. P., Stark D. P., 2014, ApJ, 795, 20
Senchyna P., Stark D. P., Vidal-García A., et al., 2017, preprint, (arXiv:1706.00881)
Shibuya T., et al., 2017a, preprint, (arXiv:1704.08140)
Shibuya T., et al., 2017b, preprint, (arXiv:1705.00733)
Smit R., et al., 2014, ApJ, 784, 58
Smit R., Bouwens R. J., Labbé I., Franx M., Wilkins S. M., Oesch P. A., 2016, ApJ, 833, 254
Smit R., et al., 2017, preprint, (arXiv:1706.04614)
Smith A., Bromm V., Loeb A., 2016, MNRAS, 460, 3143
Sobral D., Best P. N., Smail I., Mobasher B., Stott J., Nisbet D., 2014, MNRAS, 437, 3516
Sobral D., Matthee J., Darvish B., Schaerer D., Mobasher B., Röttgering H. J. A., Santos S., Hemmati S., 2015, ApJ, 808, 139
Sparre M., Hayward C. C., Feldmann R., Faucher-Giguère C.-A., Muratov A. L., Kereš D., Hopkins P. F., 2017, MNRAS, 466, 88
Stanway E. R., Eldridge J. J., Becker G. D., 2016, MNRAS, 456, 485
Stark D. P., Ellis R. S., Chiu K., Ouchi M., Bunker A., 2010, MNRAS, 408, 1628
Stark D. P., et al., 2015, MNRAS, 454, 1393
Stark D. P., et al., 2017, MNRAS, 464, 469
Taylor M., 2013, Starlink User Note, 253
Tilvi V., Pirzkal N., Malhotra S., et al., 2016, ApJ, 827, L14
Treu T., Schmidt K. B., Trenti M., Bradley L. D., Stiavelli M., 2013, ApJL, 775, L29
Van Der Walt S., Colbert S. C., Varoquaux G., 2011, Computing in Science & Engineering, 13, 22
Veilleux S., 2002, in Green R. F., Khachikian E. Y., Sanders D. B., eds, Astronomical Society of the Pacific Conference Series Vol. 284, IAU Colloq. 184: AGN Surveys. p. 111 (arXiv:astro-ph/0201118)
Venemans B. P., et al., 2012, ApJL, 751, L25
Visbal E., Haiman Z., Bryan G. L., 2016, MNRAS, 460, L59
Watson D., Christensen L., Knudsen K. K., Richard J., Gallazzi A., Michałowski M. J., 2015, Nature, 519, 327
Wilkins S. M., Bouwens R. J., Oesch P. A., Labbé I., Sargent M., Caruana J., Wardlow J., Clay S., 2016, MNRAS, 455, 659
Zheng Z.-Y., et al., 2017, ApJL, 842, L22
de Barros S., Schaerer D., Stark D. P., 2014, A&A, 563, A81

APPENDIX A: REDUCED DATA: PUBLIC RELEASE

We publicly release all spectroscopic and imaging data described and analysed in this paper. This includes the 2Ds from X-SHOOTER and HST/WFC3, along with the flux calibrated SINFONI data-cubes. We also release our extracted 1D spectra, flux calibrated, including our best estimate of the $1\,\sigma$ noise per wavelength element. We release these as fits files, available to download with the refereed paper. Raw data are also publicly available for all the datasets described here by querying the appropriate archives and proposal IDs.

APPENDIX B: VARIABILITY IN ULTRAVISTA

In order to understand the puzzling flux differences in the J band for CR7, we check how the magnitude of CR7 has changed in the 3 data releases of the UltraVISTA survey. We retrieve catalogues from the ESO archive and include all sources that are 1: detected in all UltraVISTA data releases and 2: within 5 arcmin separation from CR7. CR7 itself is only detected in all three releases in the Y and J bands. DR1 was released in February 2012, while DR2 was released in January 2014 and DR3 in April 2016. While DR1 has an average exposure time of $\sim$ 50 ks (including the deep stripes), the DR2 exposure time at the location of CR7 is 46 ks. DR3 does not seem to have added any exposure time to the region where CR7 is found, with DR3 listing a total exposure time of 44.6 ks, down from 46 ks in DR2. Therefore, and according to the DR2 and DR3 release documents, the difference between DR2 and DR3 are to do with the reduction method and not in additional observations. We use aperture photometry in $1''$, $2''$ and Mag-auto and show the results in Figure B1 and Table B1.

Table B1. Variability check in UltraVISTA. No significant variability is detected, although we note that the J band magnitude in DR2 (used in Sobral et al. 2015) was boosted by 0.1-0.5 dex (depending on the aperture) with respect to DR3. This led to an over-estimate of the HeII line-flux, as J band photometry was used to calibrate the spectrum.

Colour	Aperture	Δ mag	Δ mag$_{\rm err}$	Significance
J DR3-DR2	mag-auto	0.508	0.303	1.7σ
J DR3-DR2	$r = 0.5''$	0.338	0.262	1.3σ
J DR3-DR2	$r = 1.0''$	0.125	0.299	0.4σ
J DR1-DR2	mag-auto	-0.051	0.313	-0.16σ
Y DR3-DR2	mag-auto	0.117	0.298	0.4σ
Y DR3-DR2	$r = 0.5''$	0.007	0.262	0.0σ
Y DR3-DR2	$r = 1.0''$	-0.034	0.291	-0.1σ
Y DR1-DR2	mag-auto	0.128	0.306	0.4σ

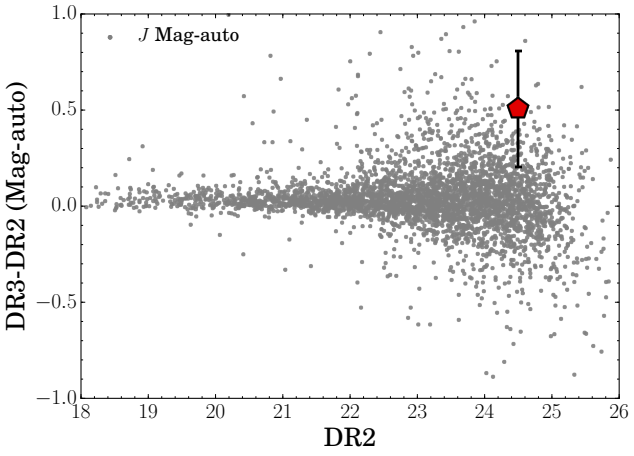


Figure B1. Comparison between mag-auto UltraVISTA J DR3 and DR2, sources within 5 arcmin of CR7. CR7 in shown red and compared to all other sources in grey.

This paper has been typeset from a TEX/LATEX file prepared by the author.